REPORT DOCUMENTATION PAGE

Form Approved
OMB No. 0704-0188

1. AGENCY USE ONLY *(Leave blank)*	2. REPORT DATE	3. REPORT TYPE AND DATES COVERED
	25.Jun.02	THESIS

4. TITLE AND SUBTITLE
A SATELLITE-BASED MULTI-CHANNEL APPROACH TO TROPICAL CYCLONE INTENSITY ESTIMATION USING THE AMSU PASSIVE MICROWAVE SENSOR

5. FUNDING NUMBERS

6. AUTHOR(S)
CAPT KABAT BRIAN W

7. PERFORMING ORGANIZATION NAME(S) AND ADDRESS(ES)
UNIVERSITY OF WISCONSIN MADISON

8. PERFORMING ORGANIZATION REPORT NUMBER

CI02-142

9. SPONSORING/MONITORING AGENCY NAME(S) AND ADDRESS(ES)
THE DEPARTMENT OF THE AIR FORCE
AFIT/CIA, BLDG 125
2950 P STREET
WPAFB OH 45433

10. SPONSORING/MONITORING AGENCY REPORT NUMBER

11. SUPPLEMENTARY NOTES

12a. DISTRIBUTION AVAILABILITY STATEMENT
Unlimited distribution
In Accordance With AFI 35-205/AFIT Sup 1

12b. DISTRIBUTION CODE

13. ABSTRACT *(Maximum 200 words)*

20020702 024

14. SUBJECT TERMS

15. NUMBER OF PAGES
63

16. PRICE CODE

17. SECURITY CLASSIFICATION OF REPORT	18. SECURITY CLASSIFICATION OF THIS PAGE	19. SECURITY CLASSIFICATION OF ABSTRACT	20. LIMITATION OF ABSTRACT

A SATELLITE-BASED MULTI-CHANNEL APPROACH TO TROPICAL CYCLONE INTENSITY ESTIMATION USING THE AMSU PASSIVE MICROWAVE SENSOR

by

BRIAN W. KABAT

A thesis submitted in partial fulfillment of the requirements
for the degree of

MASTER OF SCIENCE

(Atmospheric and Oceanic Sciences)

at the

UNIVERSITY OF WISCONSIN-MADISON

2002

Approved: _Steven Ah_ _____

Steven A. Ackerman

Professor, Department of Atmospheric & Oceanic Sciences

Date: ___4/6/02_____

Approved: _Chris Velden_ _____

Christopher S. Velden

Scientific Advisor, UW-CIMSS

Date: ___06Apr02_____

A SATELLITE-BASED MULTI-CHANNEL APPROACH TO TROPICAL CYCLONE INTENSITY ESTIMATION USING THE AMSU PASSIVE MICROWAVE SENSOR

Brian W. Kabat
Under supervision of Professor Steve Ackerman

ABSTRACT

In tropical cyclones, a strong inverse relationship exists between the magnitude of the upper-tropospheric warm anomaly (UTWA) and minimum sea level pressure (MSLP). Uniquely poised to capture this warming aloft, the Advanced Microwave Sounding Unit (AMSU) flown aboard current National Oceanic and Atmospheric Administration (NOAA) polar-orbiting satellites is capable of observing Tropical Cyclones (TCs) worldwide.

A physical/statistical MSLP estimation algorithm based on AMSU brightness temperature anomalies (dTbs) has been operating in an experimental mode at the University of Wisconsin Cooperative Institute for Meteorological Satellite Studies (UW-CIMSS) for two years. The algorithm relies on a single AMSU channel (54.9 GHz) and shows great promise as a viable TC analysis tool. However, the radiances can be susceptible to environmental variability leading to sub-sampling and errors in MSLP. The goal of this research is to improve the existing single-channel algorithm by introducing an additional channel (55.5 GHz) that seeks to capture the true magnitude of the UTWA in instances when the single channel fails. By implementing the multi-channel approach, the goal is to create an operationally viable satellite-based guidance tool to help support tropical forecast and analysis centers worldwide.

The multi-channel algorithm is developed from a dataset that includes 49 TC cases from 1999-2000. Each case consists of an AMSU-measured UTWA and an in situ MSLP measurement from reconnaissance aircraft. An independent dataset is used to test the algorithm and includes 64 TC cases from 2001. Results indicate the multi-channel algorithm significantly reduces the mean error and standard deviation of the single-channel MSLP estimates by 1.4 hPa and 1.9 hPa, respectively. This improvement is most notable during periods of deep convection, when the 54.9 GHz channel is adversely affected by hydrometeor scattering. Algorithm improvement is demonstrated through four case studies. In addition, environmental variability effects are examined, and possible qualitative analysis applications of AMSU data are presented.

Acknowledgements

I would like to thank my family first and foremost. Kim, your patience and understanding were critical in getting me to this point. Thank you for having a sense of humor! Ashley, and no offense to any future siblings, you are the highlight of my grad school experience. I love you both very much. I am proud to serve in the greatest Air Force in the world, and I appreciate the opportunities they have given me to further my education. In particular, thank you to the U.S. Air Force Academy Department of Physics for sponsoring this Master's program. I can't wait to join the team. I especially wish to express my thanks to 'Professor' Chris Velden for giving me the opportunity to explore the magnificent phenomenon of tropical cyclones as a member of his Cooperative Institute for Meteorological Satellite Studies (CIMSS) research team. His patience, guidance, and understanding were quintessential in getting me through the program under very strict time constraints. To my committee: Professors Steven Ackerman, Grant Petty, and Jon Martin, I appreciate your willingness to provide insightful feedback. Thanks for getting me through the program in time...I know it wasn't easy. Kurt Brueske, this wouldn't have happened without your endeavors. Thank you for laying the groundwork. We gratefully acknowledge the support of our research sponsors, the Office of Naval Research, Program Element (PE-060243N) and the Oceanographer of the Navy through the program office at the Space and Naval Warfare Systems Command, PMW-155 (PE-0603207N).

"Hurricane intensity is another one of those slippery problems in weather science. As the saying goes among researchers, it is not well understood. The speeds of the winds always seem to be changing–slowing down here and now, speeding up there and then. Sometimes weather scientists can point to such things as changes in ocean surface temperatures as explanations for these shifts in wind speeds. Other times, they don't have a clue."

–John D. Cox, *Weather for Dummies*, p. 161

Table of Contents

List of Tables

List of Figures

List of Attachments

1. Introduction

Over the past three decades extensive research has examined tropical cyclone (TC) intensity estimation using meteorological satellites. As the quality, reliability, and availability of the data improved, objective techniques were developed to predict storm intensity. The most widely-used TC intensity estimation and position analysis techniques employed by operational forecasters utilize infrared (IR) and visible (VIS) satellite imagery (Dvorak 1984, Velden and Olander 1998). While these products provide invaluable information about the overall structure and strength of a tropical system, they often cannot penetrate clouds to ascertain low-level storm structure. Certain wavelengths of microwave (MW) energy, on the other hand, are able to penetrate ice clouds (such as cirrus) and offer a unique perspective into TC structure. Used in concert with existing IR and VIS techniques, microwave techniques may offer that "missing piece" of information when diagnosing TC position and intensity.

The motivation behind this research is to improve an existing technique based on passive MW observations in order to provide operational forecasters with more accurate tropical cyclone intensity estimations. This study builds on work done by Velden (1982), Velden (1989), Velden et al (1991), Merrill (1995) and Brueske (2001) and exploits the multi-spectral capabilities of the Advanced Microwave Sounding Unit (AMSU), an instrument package currently flown on NOAA polar-orbiting satellites. While Brueske (2001) included the use of a single AMSU channel to predict MSLP, this study introduces a second AMSU channel to examine its contribution toward improving TC intensity estimation.

The principle unique observing capability of the AMSU is the ability to capture the upper-level warm core structures which define and support the intensity of TCs. AMSU-observed temperature anomalies were measured and recorded during the 1999 and 2000 seasons and correlated to near-concurrent in situ minimum sea level pressures (MSLP). A statistical relationship was developed and used to predict TC intensities during the 2001 season. The results were verified by reconnaissance aircraft MSLP. In addition, a preliminary study was conducted to determine the effect of incorporating ancillary data on TC eyesize and environmental sea level pressures into the AMSU algorithms in an attempt to further improve on the tropical cyclone intensity estimates. The automated algorithm ultimately generates a text-formatted intensity estimate which is derived in near-real time. This information is currently exported to forecast and analysis centers worldwide for their evaluation on an experimental basis.

This thesis shows that inclusion of a second AMSU channel (55.5 GHz) into the pre-existing algorithm improves the overall performance. In addition, supplementing AMSU data with eyesize, position, and environmental analysis information further enhances performance. Based on these results, this study demonstrates how inclusion of AMSU data in an operational setting positively impacts the overall TC analysis process.

2. Background

2.1. Tropical Cyclone Structure and Energetics

A tropical cyclone is a quasi-axially symmetric system characterized by a surface low pressure center (eye) with spiral bands of organized deep convection converging inward toward the storm center. In well-developed systems, a concentrated ring of convective thunderstorms surrounds the eye (eyewall). Horizontally, TCs range in diameter from 100 km or less to well over 1000 km. Vertically, they may occupy nearly the entire column of the troposphere to depths in excess of 15 km. Upper-levels are characterized by localized high pressure, which contributes to radial outflow aloft.

As air in the lowest levels is drawn inward toward the eye, water vapor and enthalpy fluxes from the relatively warm sea surface increase its equivalent potential temperature. Mass continuity principles imply upward vertical motion near the storm center, resulting in a thermally direct circulation on the storm scale. The relatively warm and moist inflow concentrates localized sensible heating in the eye and also contributes to additional heating throughout the remainder of the column as the air ascends in the eyewall, and condensation ultimately results in the release of latent heat.

The above thermodynamic processes, in conjunction with subsidence in the eye, tend to concentrate sensible and latent heat culminating in an upper tropospheric warm anomaly (UTWA). The inertial stability and vertical consistency of a well-developed TC tend to constrain the UTWA to a horizontal scale on the order of the radius of maximum winds. Figure 1 depicts the three-dimensional idealized UTWA.

UTWA

3 Rotation retains heat
above surface low

2 Energy liberated
through condensation

Up

1 Energy acquired
through evaporation
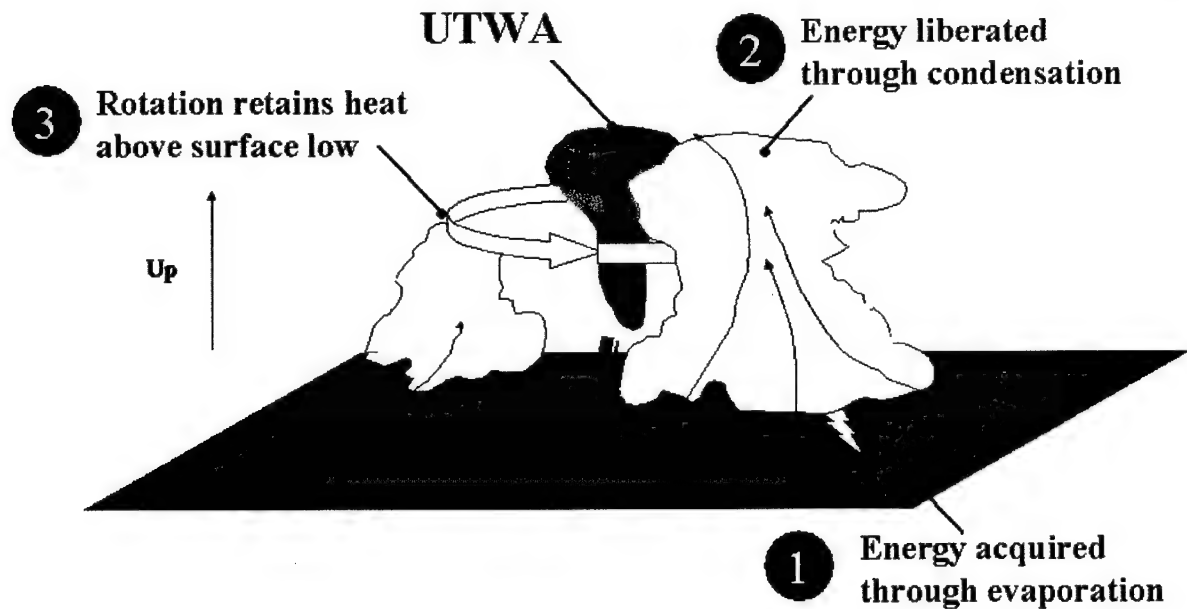
Figure 1. Idealized schematic of thermodynamic processes responsible for producing the UTWA above mature TC's. *From Brueske 2001.*

Decreasing minimum sea level pressure (MSLP) in the eye increases the TC wind field, and the drop in surface pressure (ΔMSLP) is hydrostatically linked to the magnitude of the UTWA. Velden and Smith (1983) showed the relationship between the UTWA and ΔMSLP to be nearly linear. Using hydrostatic and ideal gas constraints, this relationship can be expressed as:

$$\Delta MSLP \approx -K(\Delta \overline{T}) \qquad (1)$$

where $\Delta \overline{T}$ is the mean temperature anomaly throughout the column and K is a constant dependent on the depth of the perturbed environment and the environmental surface pressure. Thus, a positive temperature anomaly results in a low MSLP anomaly at the surface.

The existence of the UTWA has been consistently observed since the advent of aircraft penetrations of TC eyes during WWII (Fuller 1990). Temperature anomalies in the warm core have been measured with magnitudes upwards of 10-15 K in well-developed storms. Historically, vertical cross-sections of in situ TC thermal profiles have shown that maximum warming is typically concentrated near 250 hPa (34,000 ft). Figure 2 shows a temperature cross-section observed by a series of aircraft penetrations, which is strikingly similar to the idealized theoretical UTWA described above.
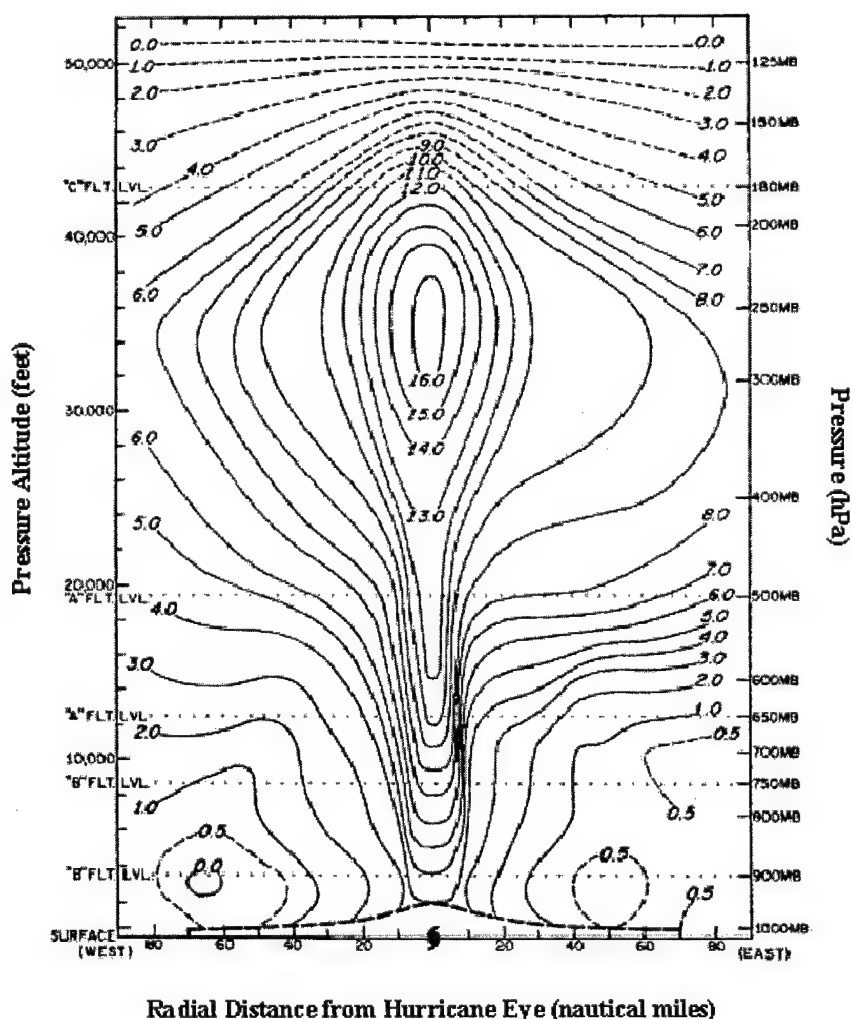
Figure 2. Cross section of temperature anomalies (K) through Hurricane Hilda (1964). *Source: Hawkins and Rubsam (1968).*

2.2. Satellite Reconnaissance of Tropical Cyclones

Due to the ferocity of TCs and their ability to impact populations and military and commercial operations, diagnosing storm intensity is critical in order to mitigate property damage and loss of life prior to landfall. Ideally, in situ sensors (whether airborne, shipborne, fixed on land, or buoys) usually provide the best overall estimation of TC intensity. As the following section will show, however, satellite data provide valuable coverage in lieu of in situ sensors.

Although in situ observations are feasible in populated areas or along heavily traveled shipping routes, for adequate warning purposes TC intensity must be diagnosed long before at-risk areas are affected. Even in the Atlantic (ATL) and occasionally Eastern North Pacific (EPAC) ocean basins, where the United States Air Force (USAF) and National Oceanic and Atmospheric Administration (NOAA) aircraft units fly scheduled surveillance missions into TCs, reconnaissance is often cost ineffective and unnecessarily places aircrews at risk unless the storm will potentially impact populated areas. There are currently no such missions in the Northern West Pacific (NWPAC) or Indian Ocean (IO) basins.

TCs form and often travel for thousands of kilometers in the data-sparse oceans before they encounter in situ sensors. Thus, unless a TC trajectory directly intersects an in situ sensor, it may be impossible to determine storm intensity without the use of remote sensing satellites. Meteorological satellites are ideally suited for monitoring the strength and movement of TCs on a global scale. Both geostationary (GEO) and low earth orbiting (LEO) platforms have unique characteristics which enable them to contribute to the overall TC reconnaissance mission.

GEO satellites afford analysts an overview of the synoptic regime encompassing a TC which may have implications on intensity trends and forecast positions. Multi-spectral analysis of visible and infrared wavelengths allows continuous 24-hour monitoring of the tropics. LEO satellites enable forecasters to more closely examine the TC environment at higher spatial resolution and offer sensors with broader spectral ranges.

Due to their relatively low orbit (~833 km), LEOs are able to actively and passively sense lower-energy microwave (MW) radiation at the longer wavelength end of the electromagnetic (EM) spectrum. This capability allows forecasters and analysts to exploit temperature and moisture sounding of specific atmospheric gases currently unattainable using higher-orbit (~36,000 km) GEOs. Unfortunately, temporal resolution of an individual LEO satellite and horizontal coverage of the tropics are inferior due to orbital geometry. The NOAA-KLM series LEOs operate on a sun-synchronous schedule: the satellite passes over a particular location on the Equator twice at the same local time each day; once on an ascending pass (toward the North Pole) and once on a descending pass (toward the South Pole). Thus, a TC may only be captured up to twice daily by each satellite depending on its location relative to the center of the overpass. Since this study utilizes two NOAA-KLM satellites (NOAA-15 and NOAA-16), we may achieve up to four passes per day over a particular system.

On occasion, TCs are not suitably located for capture by the NOAA overpass. Due to the limited swath width (~2300 km) of the NOAA-KLM series, successive orbits are not always overlapping, particularly close to the Equator. Figure 3 depicts a 24-hour period on 12 March 2002. AMSU 54.9 GHz temperatures for each descending pass are shown in the brightly colored swaths with red indicative of relative warming. The black "gaps" in AMSU

coverage highlight the sensor's limited coverage in the Tropics. In this particular example Cyclone 18S (Hary), represented by the bright red warm anomaly (UTWA) just east of Madagascar, was located on the edge of two consecutive descending passes. Although extremely rare, the degraded coverage in the Tropics may not yield any usable passes from an individual satellite for up to two days.
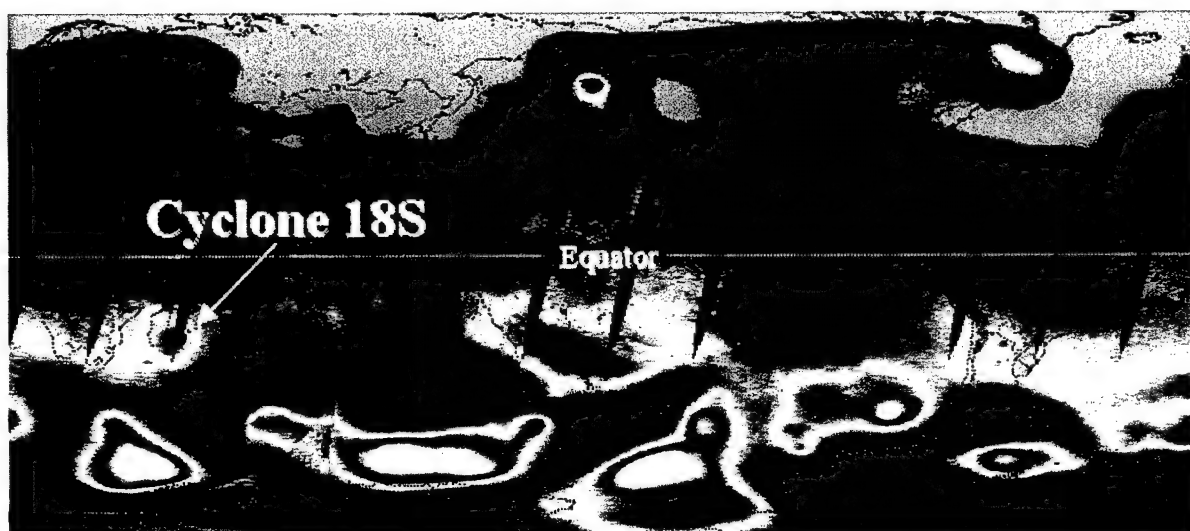
Figure 3. AMSU 54.9 GHz channel descending pass coverage for a 24-hour period on 12 March 2002. Relatively warm temperatures are depicted in red. In this example, Cyclone 18S (Hary) is located on the edge (limb) of two successive orbits with the UTWA falling prey to poor data coverage in the Tropics. *Source: NASA Marshall Space Flight Center Passive Microwave Earth Science Information Partner website: http://pm-esip.msfc.nasa.gov/amsu/index.phtml*

As TCs move toward higher latitudes, coverage by LEO satellites improves, particularly poleward of 30° where AMSU passes begin to overlap. Consequently, a TC may be captured by two successive AMSU passes. Theoretically, the two AMSU instruments may capture a TC up to eight times each day in these circumstances. More typically though, users can

expect anywhere from 2-4 AMSU passes daily over a TC located in very low latitudes and 4-6 passes at higher latitudes.

Operational forecast centers, including the National Hurricane Center (NHC), Joint Typhoon Warning Center (JTWC), and Air Force Weather Agency (AFWA) are responsible for TC warning and forecasting for designated oceanic basins. Although most TC analysts at these centers utilize products from a wide array of satellite sensors, the accepted method of determining TC intensity when no in situ data are available is the Dvorak Technique (Dvorak 1975). This technique uses primarily enhanced infrared (IR) brightness temperatures (Tbs) and relies on a decision matrix of pattern recognition, cloud top temperatures, and trend constraints. Although extremely effective under certain conditions, it is difficult to ascertain TC thermal structure beneath the clouds, particularly in cases where lower clouds and organized convection are obscured by a broad cirrus shield. In addition, systems undergoing rapid intensity changes are often misrepresented due to Dvorak trend constraints.

The unique viewing capabilities of passive MW techniques offer a perfect complement to the well-established Dvorak Technique. Passive microwave sensors operate at low frequencies such that most ice crystals and aerosols have small effective radii when compared to the wavelength of the sensed radiation (4+ orders of magnitude). As a result, upwelling MW radiation in certain wavelengths is relatively unaffected by ice clouds, allowing analysts a view into the TC thermal and convective structure regardless of whether a cirrus shield is present.

Kidder, et al. (1978) first attempted passive microwave TC intensity estimation using the Scanning Microwave Spectrometer (SCAMS) aboard Nimbus-5 and Nimbus-6 satellites. Although a positive correlation between the UTWA and MSLP was observed, the extremely

coarse horizontal resolution severely limited the ability of the sensor to sufficiently resolve the warm core. The increased horizontal resolution of the Microwave Sounding Unit (MSU) flown aboard NOAA-6 through NOAA-14 LEO satellites offered new advantages for Velden and Smith (1983). They derived a set of linear regression coefficients that related observed brightness temperature anomalies (dTbs) with aircraft observed MSLPs. The technique was advanced in the Atlantic (Velden 1989) and Western North Pacific (Velden, et al. 1991) where a number of sensitivities (storm latitude, storm development stage, size, etc.) were examined. However, the spatial resolution of the MSU relative to the TC warm anomaly was still found to be a limiting factor. Finally, Merrill (1995) and Brueske (2001) transitioned the technique to the AMSU and also developed a method to explicitly account for subsampling and diffraction effects. Table 1 compares relevant specifications of the three sensors.

	SCAMS	MSU	AMSU-A	AMSU-B
Platforms	Nimbus-6	NOAA- 6-14	NOAA-15+	NOAA-15+
Number of Channels	5	4	15	5
Frequency Range GHz)	22.24-55.45	50.3-57.95	23.8-89.0	89.0-183.3
Wavelengths (mm)	5.41-13.48	5.17-5.96	3.37-12.6	1.63-3.37
NEΔT (K)	0.2	0.3	0.25-1.2	0.8
Beam Width	7.5°	7.5°	3.3°	1.1°
Nadir Resolution (km)	145	110	48	16

Table 1. Comparison of microwave radiometers used to monitor TC's.

The increased spatial resolution, decreased radiometric noise (NEΔT), and the additional channels in the 53-56 GHz region have significantly improved the efficacy of the AMSU in monitoring the thermal structure of TCs over its predecessors.

2.3. Microwave Remote Sensing

Microwave brightness temperatures result from an inversion of the Planck function radiance equation:

$$B(\lambda,T) = \frac{2hc^2}{\lambda^5 (e^{\frac{hc}{\lambda kT}} - 1)} \Rightarrow Tb = \frac{hc}{k} \frac{1}{\lambda \ln(\frac{2hc^2}{\lambda^5 (B(\lambda,T))} + 1)} \qquad (2)$$

where $B(\lambda,T)$ is the Planck function radiance, h Planck's constant, c the speed of light, λ the wavelength of sensed radiation, k Boltzmann's constant, T scene temperature, and Tb the equivalent blackbody temperature (brightness temperature). Although this relationship is highly non-linear at short wavelengths ($\lambda<5$mm), it becomes nearly linear in the microwave spectrum at terrestrial temperatures where $ch/\lambda<<kT$. The Planck function radiance and corresponding brightness temperature equations can then be expressed in the linear Rayleigh-Jeans approximation by substituting the expansion $e^x \approx (1+x)$ where $x=hc/\lambda kT$:

$$B(\lambda,T) = \frac{2kcT}{\lambda^4} \Rightarrow Tb = \frac{\lambda^4 B(\lambda,T)}{2kc} \qquad (3)$$

The result is a linear relationship between radiance and brightness temperature, implying that an unattenuated brightness temperature anomaly can represent the true magnitude of the UTWA. It is therefore possible to derive a linearly regressed set of coefficients that directly equate the observed AMSU temperature anomalies to physical fluctuations in MSLP.

Ideally, an integrated suite of products maximizing the benefits of each spectral band from both GEO and LEO sensors should be employed in conducting a full analysis of TCs

and their environments. Focusing on one small piece of the multi-spectral puzzle, this study examines atmospheric contributions of upwelling radiation in a portion of the strong oxygen absorption band centered near 60 GHz in the MW EM spectrum (Figure 4).
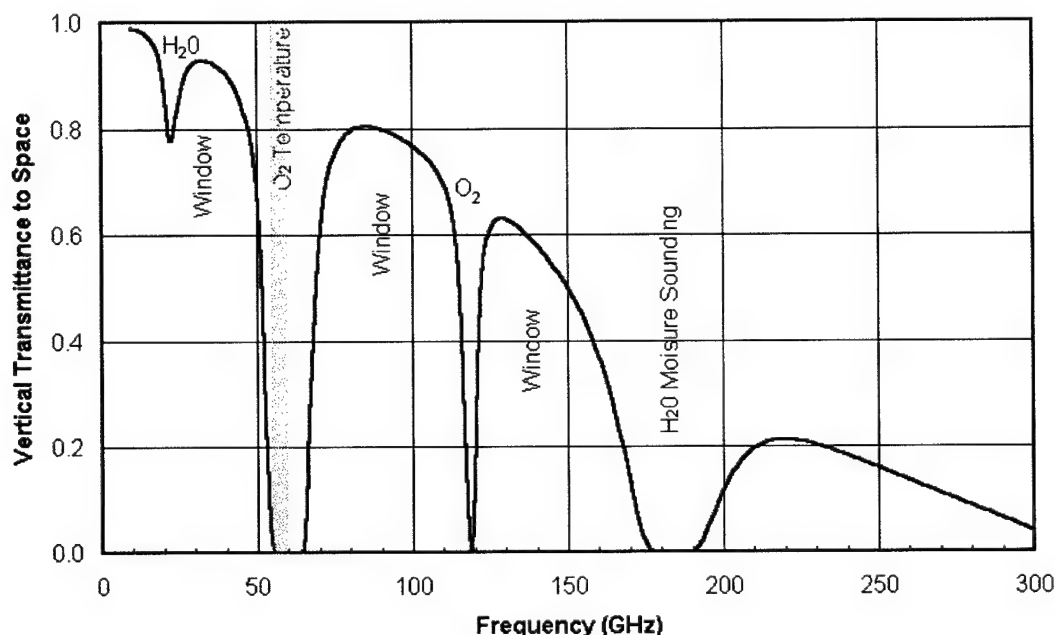
Figure 4. Microwave spectrum in the 15°N annual atmosphere. Shaded region indicates approximate spectral range of AMSU channels 5-8. *Source: Kidder et al. (2000).*

AMSU channels 1-15 (AMSU-A) are primarily utilized as temperature sounding channels, exploiting absorptive properties of specific constituents to determine characteristics of discrete layers of the atmosphere. More specifically, channels 5-8 are located in a strong oxygen absorption band (Figure 4). Channels 5 and 6 are located on the edges of the absorption band, while channels 7 and 8 are successively closer to the center of the absorption band. As a result, channels 7 and 8 have weighting functions which peak higher in the troposphere than do the weighting functions of channels 5 and 6 (Figure 5).
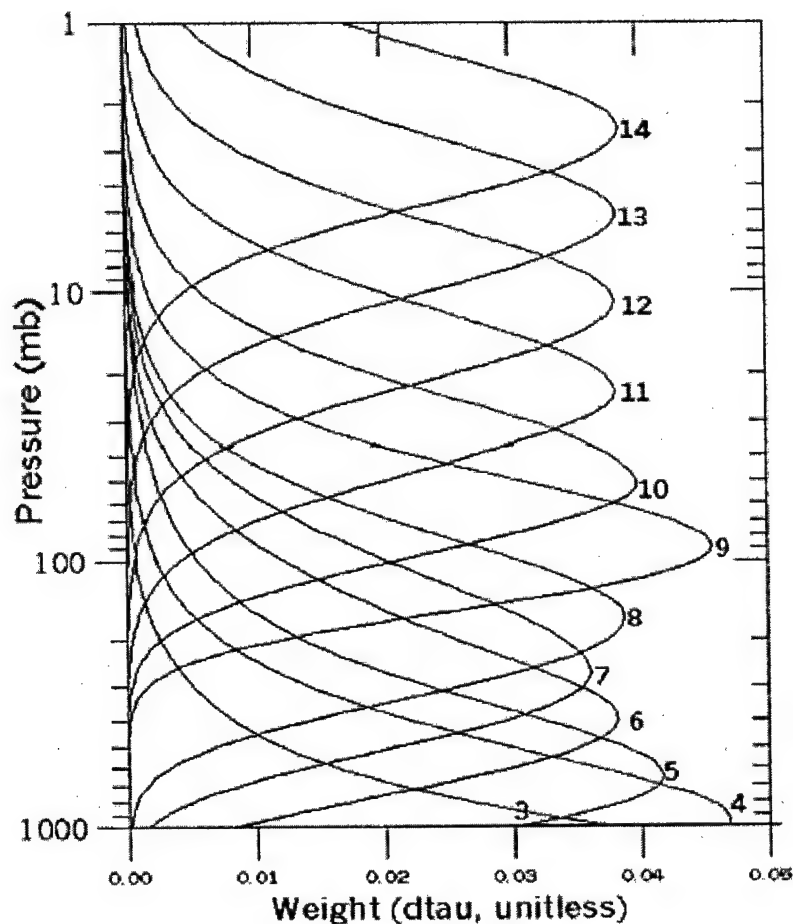
Figure 5. AMSU Weighting functions. Numbers on the right correspond to AMSU channels. Weight is a relative measure of the amount of emitted radiation at a particular pressure level contributing to the signal in that channel. *Source: Kidder et al. 2000.*

The result is a limited temperature sounding capability between the channels at four different levels in the atmosphere, with channel 7 (54.9 GHz) peaking most closely to the known climatological altitude of the UTWA (Figure 2) and channel 8 (55.5 GHz) slightly higher. Because AMSU channels 5 and 6 peak in the lower and middle troposphere, they are considerably more susceptible to contamination by liquid (raindrops, large water cloud droplets, etc.), mixed-phase (water-coated graupel, melting snow, etc.), and frozen (graupel, hail, etc.) hydrometeors associated with convection in and around the LLCC. This is

because the sensed wavelengths associated with this band (~5.5mm) are within an order of magnitude of the diameter of typical hydrometeors which are capable of scattering the MW radiation away from the AMSU sensor. Although channel 7 (~250hPa) is occasionally impacted during periods of intense convection, channel 8 is less frequently attenuated in general, since it peaks considerably higher in the troposphere. This characteristic is a key motivation for incorporating this channel into the pre-existing intensity estimation algorithm. Table 2 lists the properties of the AMSU channels relevant to this study.

AMSU Channel	Frequency (GHz)	Wavelength (mm)	Wavenumber (cm^{-1})	Nadir Resolution (km)
5	53.6	5.59	1.79	48
6	54.4	5.51	1.81	
7	54.9	5.46	1.83	
8	55.5	5.40	1.85	
16	89.0	3.37	2.97	16

Table 2. AMSU Channels 5-8, 16 characteristics. Source: *NOAA/NASA Polar Orbiting Environmental Satellite (POES) Guide, NP-1997-12-052-GSFC*.

In addition to the obvious resolution advantages over its predecessors, the AMSU also has a much broader spectral range. The 89.0 GHz AMSU-B channel 16 is located in an atmospheric absorption minimum (window) and is capable of sensing surface emission. Furthermore, it is even more susceptible to scattering (wavelength of ~3.4mm) by precipitation and suspended hydrometeors. The combined effect makes this channel ideal for determining certain LLCC properties. The relatively large droplet size of liquid water clouds often associated with TC cumulus frequently attenuate the upwelling microwave radiation in such a fashion that it is possible to discern cloud patterns in and around the eye. AMSU-B imagery is therefore an excellent diagnostic tool in assessing the location of the LLCC, and

in well-developed systems, provides a good estimate of the eyesize which is directly related to the size of the UTWA (Merrill 1995).

The AMSU is a cross-track scanning microwave radiometer, meaning that only points directly below the satellite subpoint (nadir) are sensed at optimal resolution. As scan angles increase from nadir, horizontal resolution is degraded with the signal traversing a greater depth of upper troposphere. While these effects are explicitly treated in data processing for this study (i.e., limb corrections), diffraction effects due to broadening of the antenna gain patterns with scan angle are not.

3. Data

AMSU data are received at the University of Wisconsin (UW)– Space Science and Engineering Center (SSEC) Cooperative Institute for Meteorological Satellite Studies (CIMSS) in near real time. NOAA-15 and 16 onboard communications relay raw radiance data to one of two NOAA/NESDIS Command and Data Acquisition Stations (CDAS) located in Fairbanks, AK and Wallops Island, VA where the data are subsequently processed and shipped to a telecommunications satellite for broadcast to end users. Although the time delay between AMSU observation and receipt at CIMSS can occasionally exceed four hours during periods of communications saturation, more typically data are available for internal processing within two to four hours. This rapid availability enables researchers and analysts to monitor evolving systems in near-real time.

Each time the NOAA satellites complete an orbit, AMSU data are stored in two files each containing raw radiance data for each footprint of each scan swath captured during the approximately 115 minute revolution around the earth. The first file contains data corresponding to AMSU-A (channels 1-15), and the second corresponds to AMSU-B (channels 16-21). Table 3 shows the syntax of AMSU orbit filenames.

Example AMSU Filename:	a15047s0329e0515	
Character(s)	Meaning	Example Interpretation
1	AMSU-A/B designator	This is an AMSU-A file...AMSU-B begins 'b'
2-3	Satellite number	This is a NOAA-15 satellite...NOAA-16 is '16'
4-6	Julian day	This is the 47th day of the calendar year
7-11	Orbit start time	This orbit starts (s) at 0329 UTC
12-16	Orbit end time	This orbit ends (e) at 0515 UTC

Table 3. AMSU filename structure.

Because only those data corresponding to the geophysical coordinates of the TC are pertinent, it is imperative to select the correct orbit file from the local database. Utilizing NOAA/NESDIS orbital ephemeris prediction algorithms along with analyzed and forecast positions of TCs, it is possible to interpolate between the start and end times of the orbit to extract the precise footprints for analysis from the appropriate orbit file.

In addition to AMSU observations, a number of other data sources are used in this study. Text-formatted tropical cyclone warnings issued by JTWC and NHC contain critical forecast positions and corresponding date-time groups (DTG). Aircraft reconnaissance reports available via the NHC website as well as buoy observations available through the National Buoy Data Center provide verification of MSLP used in the development and testing of the AMSU algorithm. Multi-spectral satellite imagery from the Naval Research Laboratory (NRL) provides complimentary analysis data. Real-time surface observations accessed via the Joint Air Force/Army Weather Information Network (JAAWIN) provide TC intensity information during landfall. Finally, NRL Automated Tropical Cyclone Forecasting (ATCF) system files are used to provide key ancillary parameters (TC position, environmental pressure, eyesize, etc.) in testing sensitivity to environmental variability.

In constructing viable datasets, verification criteria must be established, particularly considering the dynamic nature of TCs. In this study, observed MSLPs are only considered if they are taken within six hours before or after an AMSU observation. The entire dataset spans three years (1999-2001), three tropical basins (ATL, EPAC and NWPAC), and includes 113 AMSU passes over 28 different TCs. The dependent dataset used for algorithm development and the independent dataset used to test algorithm performance are further detailed in later sections.

4. Methodology

4.1. Background

The original UW-CIMSS AMSU intensity algorithm (Brueske 2001) was developed on

an independent dataset (n=22) of AMSU channel 7 brightness temperature anomalies (dTb7)

consisting of cases from several TCs in 1999. Each TC position was manually scrutinized to

ensure the pixel associated with maximum UTWA magnitude was captured. Coincident

observed MSLPs were recorded and linear correlation coefficients were developed

(Figure 6).

1999 Atlantic Season Results
NOAA-15 AMSU-A Ch7 (54.94GHz) Tb vs. Reconnaissance Estimated MSLP
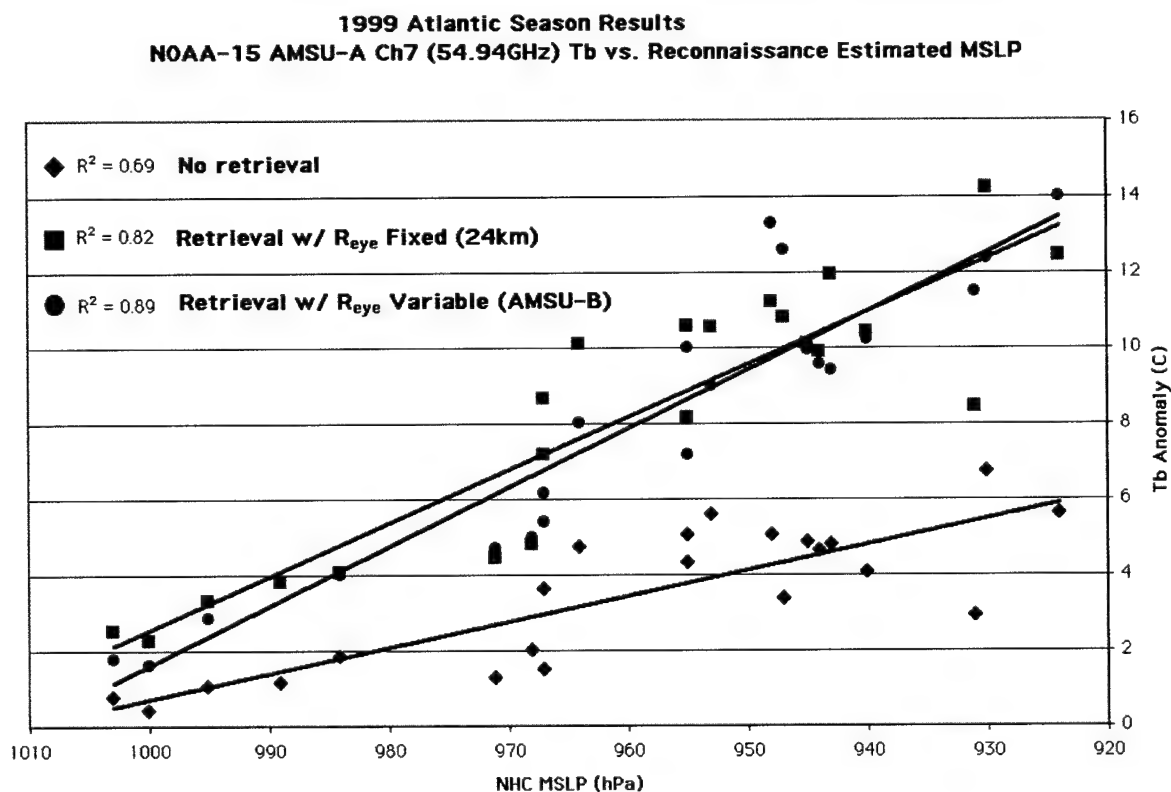
Figure 6. Results of the 1999 dependent test. Application of the retrieval increases the resolved UTWA and improves correlation with MSLP determined by aircraft. *Source: Brueske 2001.*

In addition to the correlation found between dTb7 and MSLP (referred to as the 'raw' estimates), a convolution of the antenna gain pattern, scan geometry and diffraction effects were taken into account as prescribed by Merrill (1995). A forward model (referred to as the 'retrieval') was defined in order to correct for inherent UTWA sub-sampling due to these effects. Eyesize dependent UTWA horizontal scale was also factored in. The resultant dTb and MSLP (referred to as 'retrieved' estimates) were theoretically more representative of the actual overall magnitude of the UTWA, thus minimizing the limitations of AMSU's resolving power (Figure 6).

The algorithm was applied to an independent dataset (n=31). Results appear in Table 4. Not only was there a strong correlation between UTWA magnitude and observed MSLP, but the algorithm (especially the retrieval) demonstrated significant promise as a predictive tool with standard deviations comparable to Dvorak estimates for that year (2000).

	AMSU Raw UTWA	AMSU Retrieved UTWA	NHC Dvorak estimates
MSLP correlation coefficient	0.80	0.95	-
MSLP standard deviation	9.9 hPa	8.0 hPa	7.6 hPa

Table 4. Results of the independent test of the UW-CIMSS TC intensity algorithm as compared to Dvorak pressure estimates performed by NHC Tropical Analysis and Forecast Branch (TAFB) in 2000. Based on 31 cases.

4.2. Horizontal Scale of the UTWA

As indicated in Table 4, retrieval estimates outperformed raw estimates as anticipated. Within the retrieval, scan and diffraction effects were explicitly treated, and a more realistic representation of the warming emerged. In addition to the UTWA magnitude, the horizontal scale over which the warming occurs is important in correcting for the relatively coarse spatial resolution (48 km at nadir) of the instrument. Merrill (1995) explicitly accounted for this resolution limitation using a shape parameter to determine a retrieved MSLP. Merrill (1995) and Brueske (2001) both concluded that accounting for eyesize in the retrieval dramatically improved intensity estimates.

The current retrieval developed by Brueske utilizes the higher-resolution AMSU-B channel 16 (89.0 GHz) moisture sounder to estimate TC eyesize which is subsequently used as a proxy for UTWA horizontal scale. Since 89.0 GHz radiances are strongly attenuated by precipitation, the highest radiances (warmest Tbs) should theoretically occur in the rain-free eye, and conversely, the lowest values (coolest Tbs) should correspond to those pixels in the strongest precipitation of the adjacent eyewall. Performing a spatial analysis of 89.0 GHz radiances over a range of different directions near the LLCC allows the determination of an average distance between inflection points, leading to an average diameter of the TC eye. Figure 7 depicts the scheme: by fitting a Newton polynomial interpolation to channel 16 radiances over a cross-section near the predicted TC center, the inflection point of the line should occur at the eyewall.
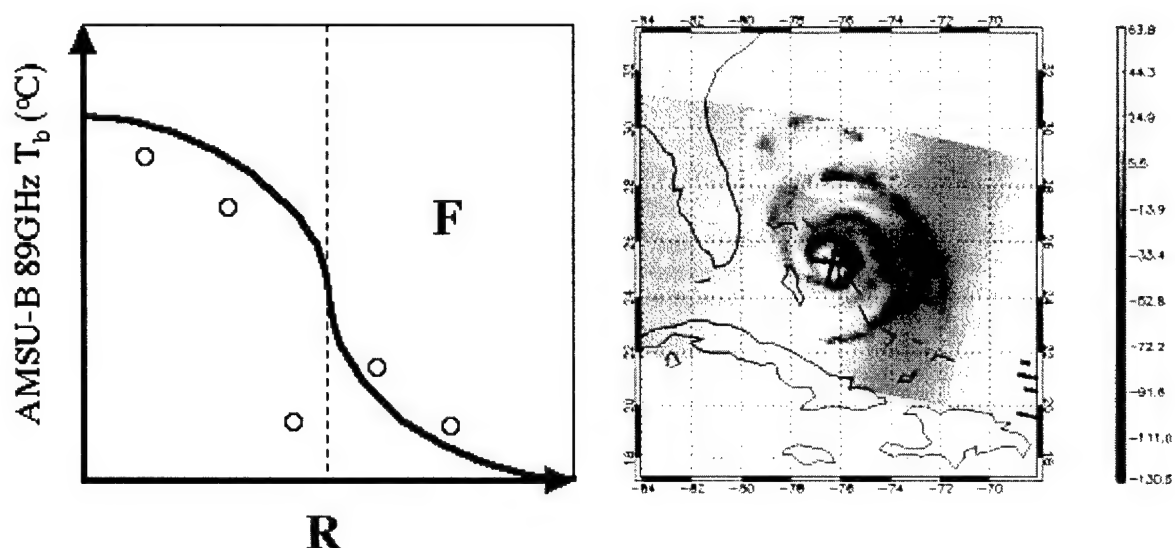
Figure 7. The retrieval algorithm horizontal size parameter is determined through spatial analysis of AMSU-B 89.0 GHz radiance data. In this example, 89.0 GHz radiances for each pixel along a radius (R) are plotted for Hurricane Floyd, 14 September 1999 at 1238 UTC, and an interpolating polynomial function (F) is assigned. The inflexion point defines a cross-over from the convective eyewall to the precipitation-free eye. This process is repeated in four directions (right) in image array line/element. Hydrometeor scattering within the eye wall region is used as an indicator of eyesize and subsequently, a proxy for UTWA horizontal scale. *Source: Brueske 2001.*

Initial tests on the 1999 dataset showed positive impact of varying TC eyesize. Referring back to Figure 6, the results of two retrieval techniques, one using a fixed eye radius of 24 km and the other using the AMSU-B-derived radius, are shown. A notable improvement is evident through the increased correlation (R^2=0.89 for AMSU-B based eyesize, versus R^2=0.82 for fixed eyesize) between retrieved UTWAs and aircraft observed MSLPs. These results represent the benchmark for the existing AMSU algorithm performance.

4.3. Single-channel UTWA Subsampling

While both the single-channel raw and retrieved estimate techniques performed comparably to Dvorak estimates during the 2000 independent test, the AMSU algorithm was based on one critical assumption: peak TC warming is adequately captured (sampled) in the single AMSU channel. However, as suggested by Brueske (2001), this assumption may be inaccurate in certain situations.

Between August and December 2001, the automated UW-CIMSS TC intensity estimation algorithm processed 817 AMSU passes over 49 TCs covering 4 tropical basins. The dTbs from both channels 7 and 8 were collected. Table 5 summarizes the apparent occurrences of UTWA subsampling in channel 7. Surprisingly, stronger warming occurred in channel 8 (dTb8>dTb7) nearly 30% of the time! Intensity estimates based solely on channel 7 in these cases would underestimate the UTWA magnitude and result in erroneously high MSLPs (intensity estimates too weak). *This finding highlights the need to expand the AMSU algorithm to a multi-channel technique.*

	All	ATL	EPAC	NWPAC	SH
n	817	245	170	350	52
n of dTb8>dTb7	242	40	48	144	10
% dTb8>dTb7	29.6	16.3	28.2	41.1	19.2

Table 5. Frequency of maximum TC core warming captured in the 55.5 GHz channel relative to the 54.9 GHz channel during 2001. n = number of cases.

At least three possible explanations have been proposed as to why the single-channel algorithm is failing to capture the UTWA peak. In each case, the second AMSU-A channel

(55.5 GHz, peak radiance contributions just above the 54.9 GHz channel) can make significant contributions toward minimizing these subsampling issues. First, vertical variations in the thermal structure exist from TC to TC (Kidder 1978). If the UTWA is peaking abnormally high or low with respect to its climatological altitude, a single channel may fail to capture the anomaly. The overlapping AMSU weighting functions (particularly in channels 7 and 8, See Figure 5) ensure that most of the signature will be captured. Secondly, as previously mentioned, precipitation contamination frequently devalues estimates based solely on dTb7s during periods of intense convection. Selecting a channel which peaks higher in the troposphere (channel 8) decreases this likelihood. Channel 8's weighting function includes less mid-tropospheric contribution, decreasing the probability of precipitation contamination effects. Thirdly, since the weighting functions are dependent on pressure and the moisture present in the atmospheric column sampled, they may not be constant from TC to TC. Thus, it is possible that the thermodynamic environment may cause the weighting function peaks to shift vertically from their climatological levels. Adding a second channel, therefore, increases the probability of capturing the UTWA. In this case, if the channel 7 weighting function peak occurs below the maximum warming, it may be captured in a lowered channel 8 weighting function peak.

4.4. Dependent Dataset and Approach

The 1999 and 2000 datasets were combined to establish a developmental dataset (n=49) which appears in Table 6. Each datapoint in the set was reexamined using the AMSU TC intensity estimation algorithm. AMSU datafiles were extracted from 8mm tape (1999) and

CD-ROM (2000) and the TC coordinates from the previous study were used to re-derive

channel 7 temperature anomalies (dTb7s). In addition, the 55.5 GHz channel 8 temperature

anomaly (dTb8) was derived in each case to determine its relationship to the TC UTWA and

possible contribution toward improving the existing single-channel algorithm. Again, this

portion of the research makes no attempt to correct the retrieval method of the AMSU
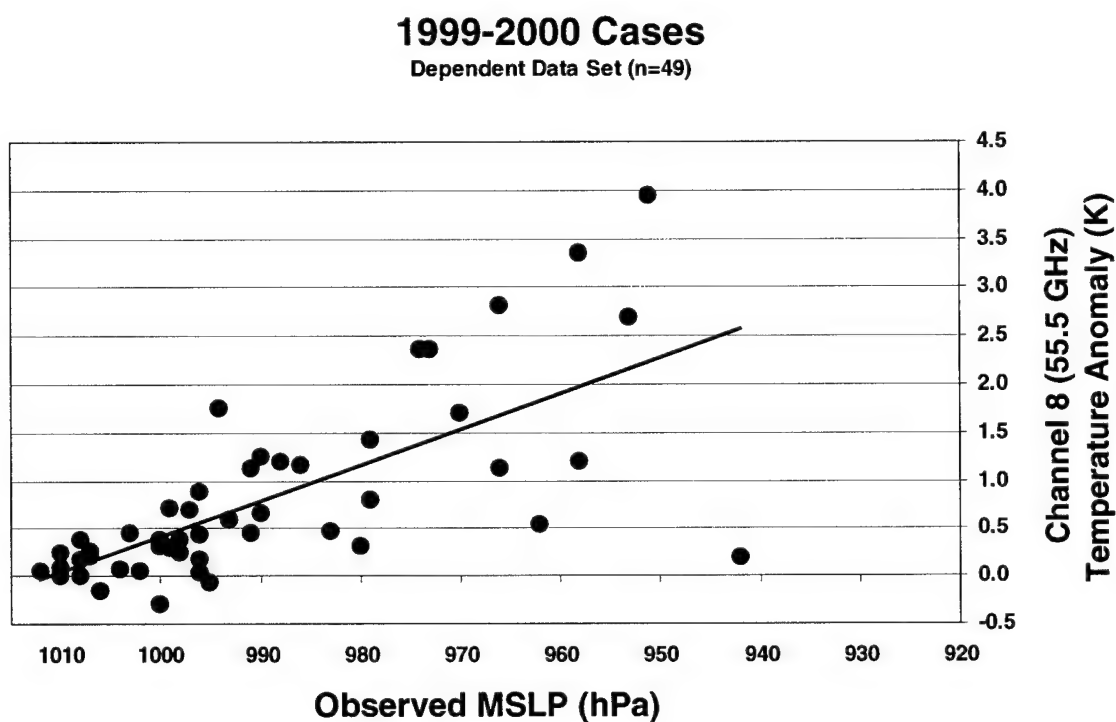
algorithm. This will be addressed in future projects.

1999-2000 Cases

Dependent Data Set (n=49)

Figure 8. Statistical relationship between AMSU 55.5 GHz brightness temperature anomalies and observed MSLP's in the dependent dataset.

Storm	Date	Basin	Observed MSLP (hPa)	AMSU (UTC)	Latitude (°)	Longitude (°)	dTb7 (K)	dTb8 (K)
Bret	20-Aug-99	ATL	1000	1:20	19.8	94.7	0.35	0.38
Bret	20-Aug-99	ATL	999	13:50	20.4	94.5	0.44	0.71
Bret	21-Aug-99	ATL	983	1:02	21.9	94.5	0.73	0.47
Bret	21-Aug-99	ATL	980	13:28	23.3	94.7	0.64	0.32
Cindy	31-Aug-99	ATL	991	11:20	39.90	48.70	1.73	0.45
Emily	26-Aug-99	ATL	1008	11:38	15.0	56.6	-0.07	0.01
Emily	26-Aug-99	ATL	1010	22:44	17.0	57.1	0.10	0.00
Emily	27-Aug-99	ATL	1010	11:14	19.0	57.0	0.12	0.09
Floyd	16-Sep-99	ATL	962	13:48	35.7	76.8	2.13	0.55
Gert	12-Sep-99	ATL	1003	10:20	14.2	31.9	0.59	0.46
Gert	12-Sep-99	ATL	996	21:26	14.8	35.5	0.94	0.89
Gert	14-Sep-99	ATL	970	11:15	16.8	44.6	1.98	1.71
Gert	15-Sep-99	ATL	951	10:54	17.5	48.9	4.12	3.95
Gert	18-Sep-99	ATL	958	22:36	23.4	58.1	3.30	3.35
Gert	22-Sep-99	ATL	973	22:52	41.8	57.0	3.73	2.37
Harvey	20-Sep-99	ATL	1002	1:38	26.3	87.4	0.46	0.05
Harvey	20-Sep-99	ATL	998	14:02	27.0	86.3	0.63	0.24
Harvey	21-Sep-99	ATL	996	1:16	27.1	84.6	0.47	0.44
Harvey	21-Sep-99	ATL	996	13:40	26.0	82.8	0.39	0.04
Debby	22-Aug-00	ATL	999	11:57	18.26	63.51	1.06	0.29
Debby	22-Aug-00	ATL	998	23:06	19.30	66.70	0.24	0.38
Debby	23-Aug-00	ATL	1006	11:32	19.86	69.26	0.25	-0.16
Debby	24-Aug-00	ATL	1012	0:24	20.00	73.40	0.10	0.06
Florence	12-Sep-00	ATL	991	12:22	30.37	73.13	1.12	1.13
Florence	14-Sep-00	ATL	995	13:15	29.46	73.52	0.74	-0.07
Gordon	14-Sep-00	ATL	1008	13:20	19.83	87.24	0.24	0.39
Gordon	17-Sep-00	ATL	990	13:50	27.27	84.05	1.03	0.66
Helene	20-Sep-00	ATL	1010	0:17	19.80	81.20	0.28	0.24
Helene	21-Sep-00	ATL	1007	14:00	26.34	87.28	0.23	0.27
Helene	22-Sep-00	ATL	1000	1:14	28.92	86.49	0.09	0.31
Joyce	01-Oct-00	ATL	1007	11:57	11.70	60.80	-0.06	0.21
Joyce	01-Oct-00	ATL	1008	23:02	11.46	62.22	0.06	0.18
Keith	29-Sep-00	ATL	1004	0:13	16.04	82.57	0.15	0.08
Keith	29-Sep-00	ATL	1000	12:42	17.22	84.49	0.42	-0.29
Keith	01-Oct-00	ATL	966	1:08	18.00	87.00	2.43	2.81
Keith	01-Oct-00	ATL	942	13:37	17.70	87.50	0.73	0.19
Keith	02-Oct-00	ATL	958	0:46	17.87	87.90	1.08	1.21
Keith	02-Oct-00	ATL	979	13:15	17.54	87.93	1.16	0.81
Keith	04-Oct-00	ATL	996	14:08	20.14	93.36	0.20	0.18
Michael	17-Oct-00	ATL	990	12:31	29.60	71.10	1.73	1.26
Michael	17-Oct-00	ATL	988	23:46	30.38	70.93	1.82	1.21
Michael	18-Oct-00	ATL	986	12:07	31.10	70.50	1.84	1.16
Michael	18-Oct-00	ATL	979	23:24	34.10	68.00	2.56	1.43
Michael	19-Oct-00	ATL	966	23:00	47.26	55.73	1.18	1.13
ST Low	26-Oct-00	ATL	997	23:42	27.50	71.50	0.75	0.69
Tembin	18-Jul-00	NWPAC	993	21:48	25.98	142.20	0.37	0.59
Saomai	12-Sep-00	NWPAC	953	10:04	26.50	128.00	2.75	2.69
Bebinca	02-Nov-00	NWPAC	994	10:51	14.43	122.67	1.45	1.76
Abigail	26-Feb-00	SPAC	974	10:46	-16.50	138.60	2.65	2.36

Table 6. Dependent dataset (n=49). ATL-Atlantic basin, NWPAC-Northern West Pacific basin, SPAC- Southern Pacific basin, dTb7-AMSU Channel 7 (54.9 GHz) temperature anomaly, dTb8- AMSU Channel 8 (55.5 GHz) temperature anomaly.

Figure 8 depicts the statistical relationship derived between dTb8s in TC cores and corresponding in situ MSLP measurements in the dependent dataset. The equation corresponding to a linear best fit to the data can be expressed as:

$$\text{MSLP}=(\text{dTb8}-37.71)/(-0.037) \qquad (4)$$

Theoretically, MSLP can be predicted based solely on dTb8s. For comparison, the equation used to estimate MSLP based solely on the dTb7-MSLP relationship can similarly be expressed as:

$$\text{MSLP}=(\text{dTb7}-65.37)/(-0.065) \qquad (5)$$

In an attempt to utilize radiance data from both channels 7 and 8, a multi-channel algorithm was developed for testing during the 2001 TC season. The new algorithm ran parallel to the existing single-channel approach. In its initial form, the multi-channel algorithm can be described as follows: For cases in which dTb7>dTb8 (n=45), MSLPs were estimated using the existing algorithm's single channel approach (Equation 5); for cases in which dTb8≥dTb7 (n=19), the new coefficients based on the 55.5 GHz channel relationship (Equation 4) were invoked to estimate a final MSLP.

5. Results: Independent Test

During the 2001 TC season, 64 AMSU passes over 10 TCs were collected within six hours of in situ MSLP observations. All cases (Table 7) occurred in the ATL and EPAC basins, and the MSLPs were verified using aircraft reconnaissance. The dataset includes TCs varying in intensity from tropical depressions with MSLPs greater than 1009 hPa and winds less than 35 knots to destructive Category 4 hurricanes with MSLPs less than 944 hPa and winds in excess of 114 knots. Some TCs eventually made landfall while others remained at sea. A few well-developed TCs like Hurricanes Erin and Michelle had discernable eyes with radii on the order of 50+ km, well within the resolving power of the AMSU instrument. Hurricanes Iris and Juliette, on the other hand, had extremely compact eyes, and UTWAs were much too small for AMSU to fully resolve.

The following subsection details the results of implementing the multi-channel approach and deals exclusively with using dTb8 in conjunction with dTb7 in estimating TC MSLP. Again, no attempt was made to adjust retrieved estimates. The goal of this research was simply to improve the raw estimate as a stepping stone to future projects that will eventually culminate in a complete multi-channel retrieval, explicitly treating scan, diffraction and precipitation effects for AMSU channels 5-8.

Storm	Date	Basin	Observed MSLP (hPa)	AMSU (UTC)	Latitude(°)	Longitude (°)	dTb7 (K)	dTb8 (K)
Chantal	17-Aug-01	ATL	1006	18:24	14.24	66.50	0.14	0.33
Chantal	18-Aug-01	ATL	1003	7:01	14.68	70.66	0.42	0.13
Chantal	18-Aug-01	ATL	1005	12:11	14.68	72.93	0.45	0.23
Chantal	18-Aug-01	ATL	1003	18:14	14.81	74.57	0.25	0.24
Chantal	20-Aug-01	ATL	1007	13:05	17.55	85.94	0.45	0.00
Chantal	20-Aug-01	ATL	1005	19:35	17.97	87.05	0.39	-0.03
Dean	22-Aug-01	ATL	1010	17:33	19.00	65.70	0.30	0.25
Erin	06-Sep-01	ATL	1013	22:46	23.62	58.37	0.06	-0.04
Erin	07-Sep-01	ATL	1008	11:11	24.86	57.6	0.07	0.08
Erin	07-Sep-01	ATL	1004	22:23	25.85	58.16	0.55	0.56
Erin	08-Sep-01	ATL	1000	6:38	26.43	58.84	0.68	0.20
Erin	08-Sep-01	ATL	994	17:58	28.22	59.46	1.07	0.87
Erin	09-Sep-01	ATL	983	6:26	30.7	61.47	2.57	1.97
Erin	09-Sep-01	ATL	979	12:04	31.57	62.41	2.50	2.17
Erin	09-Sep-01	ATL	969	17:48	32.74	62.71	3.36	2.89
Erin	09-Sep-01	ATL	969	23:20	33.57	63.18	3.28	2.79
Erin	10-Sep-01	ATL	973	17:39	35.72	64.86	3.41	2.63
Erin	10-Sep-01	ATL	972	22:58	36.19	65.42	3.83	2.58
Gabrielle	12-Sep-01	ATL	1005	18:57	25.50	85.38	0.51	0.11
Gabrielle	13-Sep-01	ATL	1000	18:46	25.35	84.47	0.82	0.37
Gabrielle	14-Sep-01	ATL	994	7:17	25.92	83.29	1.09	0.49
Gabrielle	14-Sep-01	ATL	983	13:32	27.42	82.33	1.46	1.06
Gabrielle	15-Sep-01	ATL	998	13:08	28.71	79.99	1.03	0.67
Gabrielle	15-Sep-01	ATL	999	18:26	29.78	78.84	1.10	0.31
Gabrielle	16-Sep-01	ATL	998	0:23	30.50	77.88	0.97	0.56
Gabrielle	16-Sep-01	ATL	998	6:54	30.91	76.62	0.81	0.44
Gabrielle	16-Sep-01	ATL	997	12:45	31.70	74.75	1.11	0.54
Gabrielle	16-Sep-01	ATL	993	18:16	32.08	73.39	0.96	0.89
Gabrielle	17-Sep-01	ATL	983	12:21	35.00	66.08	2.34	1.52
Humberto	21-Sep-01	ATL	1012	17:21	25.2	64.41	0.10	0.39
Humberto	22-Sep-01	ATL	998	23:22	29.8	66.51	0.70	0.45
Humberto	23-Sep-01	ATL	994	7:21	30.29	67.39	0.71	0.12
Humberto	23-Sep-01	ATL	983	23:00	32.54	67.42	0.86	0.80
Humberto	24-Sep-01	ATL	989	7:09	34.2	66.33	1.39	0.64
Humberto	24-Sep-01	ATL	992	22:38	36.56	64.58	1.13	0.86
Jerry	07-Oct-01	ATL	1007	17:49	12.03	59.20	-0.13	0.09
Michelle	31-Oct-01	ATL	1001	18:40	15.11	83.25	0.48	0.36
Michelle	01-Nov-01	ATL	1002	1:07	15.95	83.16	0.62	0.39
Michelle	01-Nov-01	ATL	997	7:16	16.44	83.42	0.48	0.25
Michelle	02-Nov-01	ATL	989	0:44	17.44	83.87	0.92	0.37
Michelle	02-Nov-01	ATL	982	7:05	17.45	83.86	0.83	0.69
Michelle	02-Nov-01	ATL	980	13:13	17.47	84.68	0.97	0.86
Michelle	03-Nov-01	ATL	957	0:22	18.64	84.06	2.12	2.27
Michelle	03-Nov-01	ATL	937	12:50	18.98	84.20	3.18	3.48
Michelle	03-Nov-01	ATL	933	19:50	19.44	83.54	2.42	2.96
Michelle	04-Nov-01	ATL	947	12:26	20.32	82.78	2.26	2.65
Michelle	04-Nov-01	ATL	949	19:40	21.97	81.33	2.47	2.55
Michelle	06-Nov-01	ATL	980	6:20	26.87	72.65	2.09	1.08
Michelle	06-Nov-01	ATL	989	17:39	28.44	67.27	0.67	-0.03
Lorena	03-Oct-01	EPAC	1004	20:16	16.66	106.33	0.32	0.36
Iris	05-Oct-01	ATL	1005	18:12	15.55	66.08	0.20	0.16
Iris	05-Oct-01	ATL	1003	23:21	16.00	67.40	0.24	-0.08
Iris	06-Oct-01	ATL	998	6:49	16.41	69.04	0.41	0.62
Iris	06-Oct-01	ATL	998	11:51	16.45	70.43	0.18	0.11
Iris	06-Oct-01	ATL	993	18:02	16.96	71.98	0.35	0.50
Iris	07-Oct-01	ATL	987	6:38	16.94	75.60	0.19	0.39
Iris	08-Oct-01	ATL	971	8:09	17.10	82.87	0.27	0.34
Iris	08-Oct-01	ATL	954	12:46	17.12	84.23	0.46	0.40
Iris	08-Oct-01	ATL	956	19:22	16.92	86.39	0.83	1.08
Juliette	24-Sep-01	EPAC	959	14:48	15.19	103.89	1.32	1.18
Juliette	24-Sep-01	EPAC	957	20:10	15.34	104.41	1.27	1.38
Juliette	25-Sep-01	EPAC	923	14:24	16.24	106.62	1.82	2.13
Juliette	27-Sep-01	EPAC	970	2:50	19.26	110.18	3.19	3.42
Juliette	28-Sep-01	EPAC	971	2:28	22.54	110.69	2.93	2.89

Table 7. Independent dataset (n=64). ATL-Atlantic basin, EPAC-Northern East Pacific basin, dTb7-AMSU Channel 7 (54.9 GHz) temperature anomaly, dTb8- AMSU Channel 8 (55.5 GHz) temperature anomaly (K).

5.1. Results of Multi-channel Implementation

Table 8 compares results between the single (current) and multi-channel (new)

approaches as described in Section 3.4.

dTb7: 54.9 GHz anomaly *dTb8: 55.5 GHz anomaly*	Current algorithm dTb7>dTb8 cases only	Current algorithm (Channel 7 only) All cases	Applying new algorithm (Two-channel) All cases
n	45	64	64
MSLP Mean Error (hPa)	8.6	11.1	9.9
MSLP Std Deviation (hPa)	8.1	11.1	10.0

Table 8. AMSU Algorithm performance on estimating MSLP during 2001. Isolating
the cases where stronger warming was observed in Channel 7 (col. 1) shows how
performance is degraded when cases where Channel 8 warming is stronger are
included (col. 2). Using both channels improves algorithm performance (col. 3).

The first column in Table 8 excludes all cases (n=19) in which the UTWA is stronger in the

channel 8 signal than in channel 7. The purpose was to demonstrate the quality of the single-

channel raw estimates before we attempt to minimize UTWA subsampling (dTb8>dTb7).

The results indicate performance was on par with 1999 results (Table 4). The entire

independent dataset includes 19 cases in which the anomaly appears stronger in channel 8.

The second column shows the results of including those cases in the existing single-channel

algorithm. Clearly, degraded performance is reflected in the increased mean MSLP error and

standard deviation. However, when the multi-channel raw estimate approach is invoked,

mean error and standard deviation are reduced.

Included in this dataset are 14 passes over Hurricanes Iris (ATL) and Juliette (EPAC),
which had extremely compact eyes on the order of 10-15 km diameter. With a maximum
horizontal resolution of 48 km, the AMSU instrument cannot resolve the full magnitude of
the TC warm anomaly. As a result, severe sub-sampling occurs in both channels. Table 9
shows the algorithm performance excluding these cases. The performance of both algorithms
improves considerably against the results in Table 8, suggesting that "small-eye" storms are
not suitable candidates for the AMSU "raw" methods due to the spatial resolution of the
sensor.

	Current algorithm	Applying new algorithm
n	50	50
MSLP Mean Error (hPa)	8.7	7.3
MSLP Std Deviation (hPa)	7.2	5.3

Table 9. Same as Table 8 excluding "small-eye" cases during
Hurricanes Juliette and Iris.

5.2. Pertinent Examples

Examining the algorithm behavior during individual TCs illustrates the full effect of

implementing the multi-channel algorithm. Four cases are presented that lend credence to

the viability of the multi-channel approach.

Intensity estimates for Hurricane Michelle appear in Figure 9. Widespread deep

convection during peak intensity (November 2-5) attenuated channel 7 Tbs leading to a
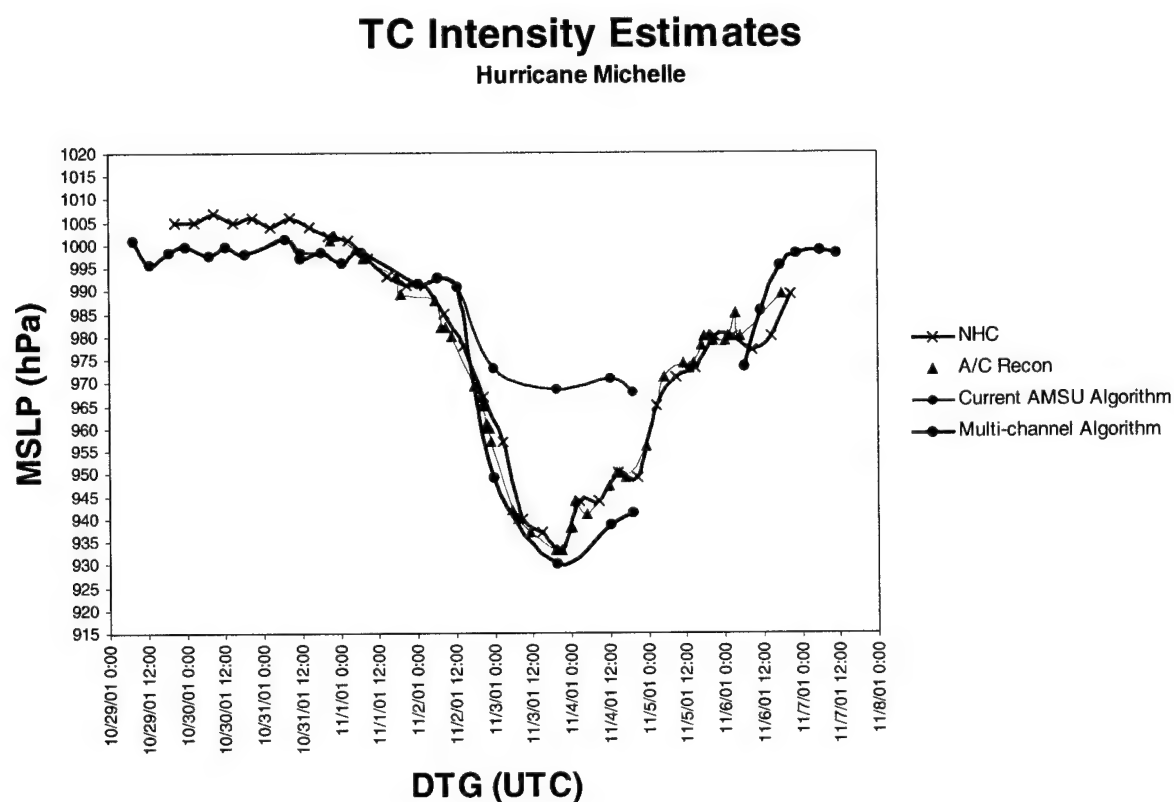
TC Intensity Estimates
Hurricane Michelle

Figure 9. Hurricane Michelle intensity estimations. NHC – National Hurricane
Center Best Track MSLP, A/C Recon – aircraft reconnaissance. The gap in data
from 5 November 0:00 to 6 November 12:00 is the result of poor AMSU
coverage (See section 2.2).

relatively poor performance of the current single-channel algorithm (blue line). During this period, Channel 8 Tbs were apparently unaffected by any precipitation attenuation. Applying the multi-channel algorithm yielded much more desirable results (red line), capturing the true UTWA magnitude when dTb8>dTb7.

Applied in the Southern Indian Ocean, the new multi-channel algorithm also makes positive contributions. Figure 10 illustrates MSLP tendencies for Tropical Cyclone 13S (Chris).

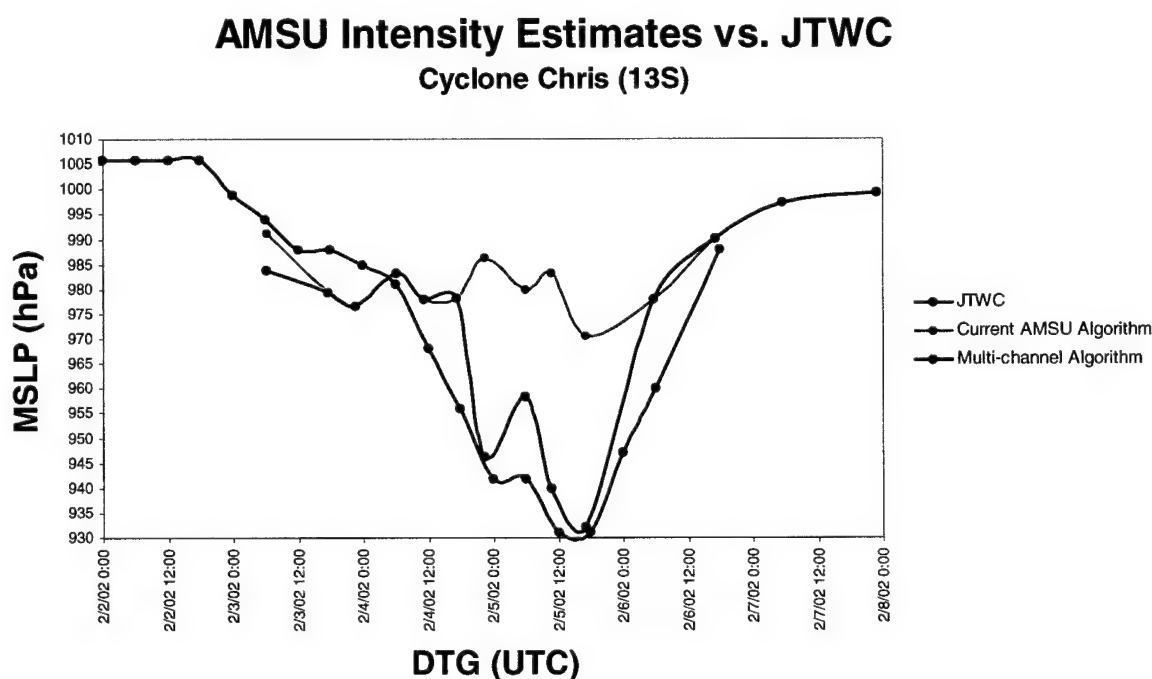**AMSU Intensity Estimates vs. JTWC**
Cyclone Chris (13S)

Figure 10. Cyclone Chris (13S) intensity estimations. JTWC – Joint Typhoon Warning Center Dvorak estimated pressures.

Cyclone Chris made landfall in a sparsely-populated area of Northern Australia between the towns of Pardoo and Wallal Downs at approximately 2020 UTC on 5 February 2002 with

winds in excess of 125 knots. When this TC came ashore, it was an intense Category 4

storm. Perth Tropical Cyclone Warning Center estimated MSLP to be near 940 hPa, while

both JTWC and the AMSU multi-channel algorithm estimated 931 and 932 hPa, respectively.

The single-channel raw estimate for the same pass (1717 UTC on the 5th) was 970 hPa.

Nearly an additional degree of warming was detected in channel 8.

One of the most intense TCs of the 2001 season was Super Typhoon Faxai (31W), a late

December storm which passed northeast of Guam. Figure 11 shows a VIS image of the TC

captured at peak intensity by the Japanese Geostationary Meteorological Satellite (GMS).

Again, inclusion of dTb8 information into the algorithm resulted in improvement as evident

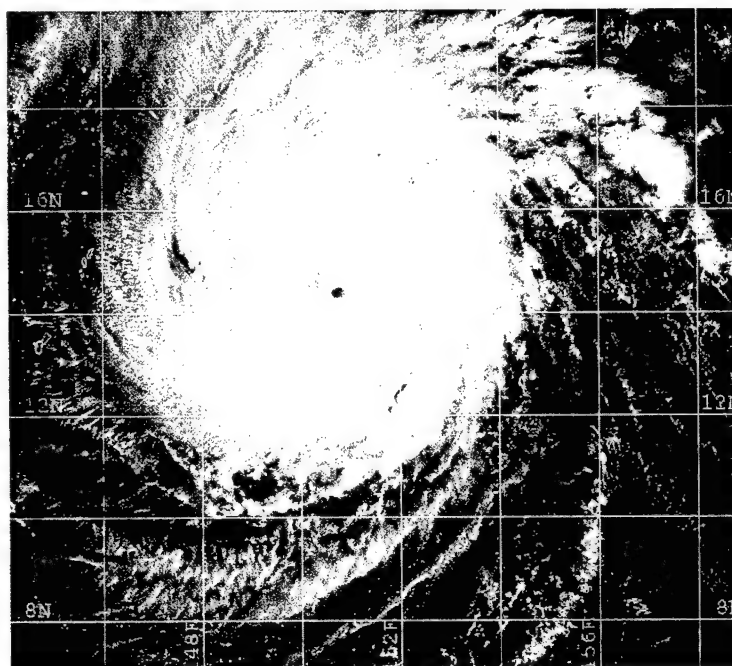in the pressure analysis shown in Figure 12.

Figure 11. GMS visible satellite imagery of Super Typhoon Faxai captured at 2131
UTC on 22 December 2001. This TC passed just east of the Northern Marianas
(seen on the left side of the image). Peak winds at the time of this image were
estimated at 155 knots with gusts to 180, which corresponds to a Dvorak pressure
of approximately 900-905 hPa. *Courtesy of Naval Research Laboratory.*

AMSU Intensity Estimates vs. JTWC
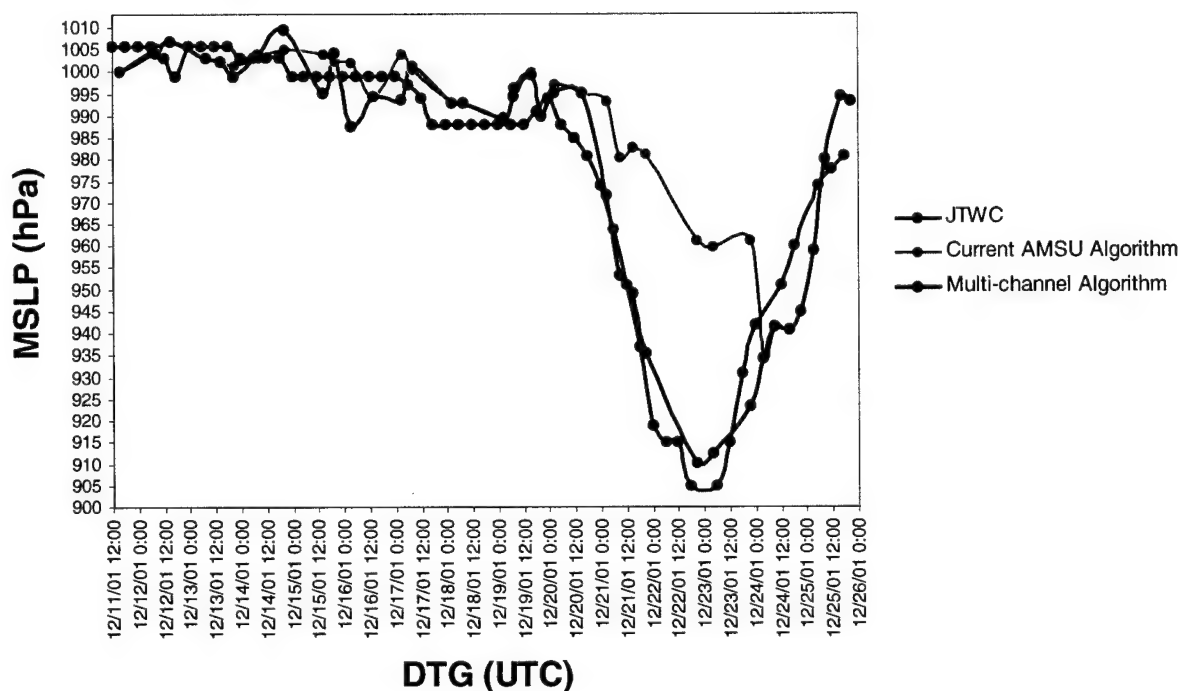### Super Typhoon Faxai (31W)

Figure 12. Super Typhoon Faxai (31W) intensity estimations. JTWC – Joint Typhoon Warning Center Dvorak estimated pressures.

Cyclone Bernie (09P) provides further evidence for infusion of AMSU MSLP estimates into a multi-spectral TC intensity analysis system. As shown in the visible satellite imagery in Figure 13, the TC passed within a few nautical miles of both Buoy 52627 stationed at 15.0° S, 139.0° E and Mornington Island weather station at 16.65° S, 139.17° E during its southward progression through the Gulf of Carpentaria. JTWC Dvorak estimates are plotted in Figure 14 along with the AMSU multi-channel algorithm estimates. In situ observations plotted during the closest point of approach seem to indicate the AMSU estimates were superior to the Dvorak technique for this case.

```
01/04/02 0000Z   09P BERNIE
01/04/02 0424Z   GMS-5 VIS
```

Naval Research Laboratory   http://www.nrlmry.navy.mil/sat_products.html
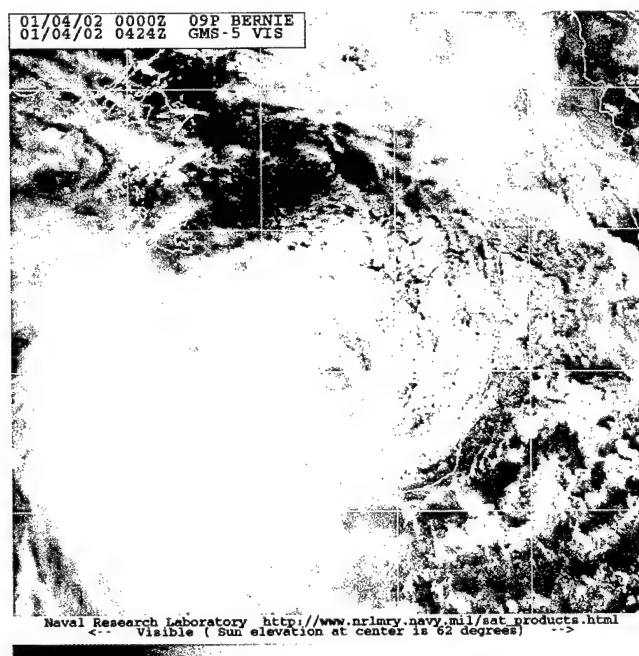<-- Visible (Sun elevation at center is 62 degrees)   -->

Figure 13. Visible imagery of Cyclone Bernie captured at 0424 UTC on 4 January 2002. The eye passed very near a permanent buoy as well as Mornington Island as it moved southward over the Gulf of Carpentaria and eventually made landfall in Northern Australia on the 5th. *Courtesy of Naval Research Laboratory.*

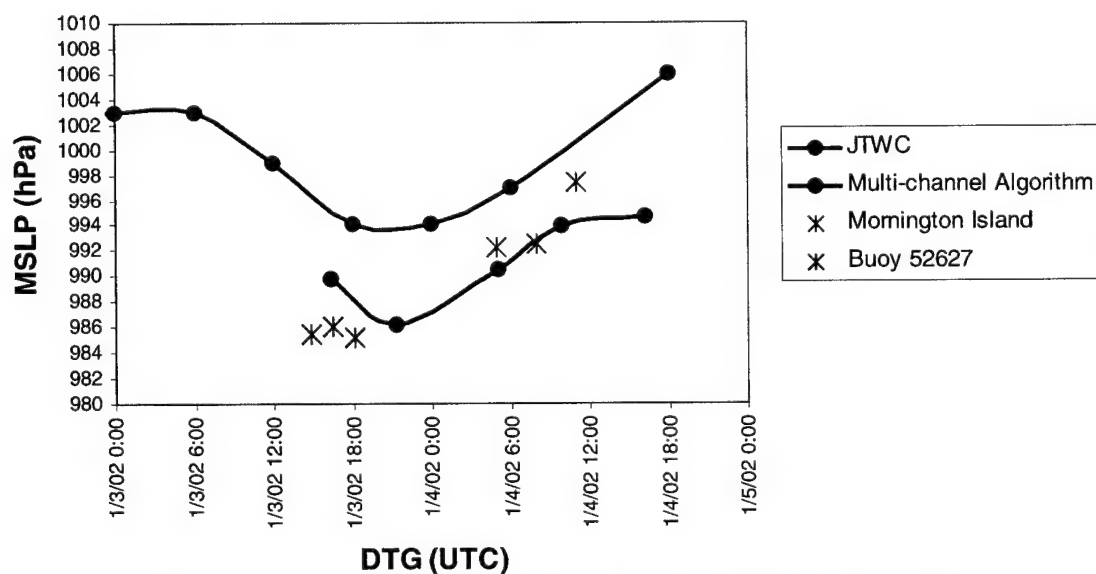## TC Intensity Estimates
Tropical Cyclone Bernie (09P)

Figure 14. MSLP estimates of Cyclone Bernie. JTWC-Joint Typhoon Warning Center Dvorak estimated pressures. In situ observations from land and buoy based meteorological sensors are also plotted.

6. Error Analysis

Although the intensity estimation scheme described in this study shows tremendous potential, significant limitations remain, particularly in the technique's current fully-automated form. Manual reanalyses of AMSU passes over TCs have shown significant improvement in certain instances. However, to be most efficiently utilized by operational forecast centers, the system needs to be as objective as possible. Understanding the sources of potential error is key to optimal utilization.

6.1. Position Error

The geographic coordinates used to determine storm position for the algorithm are primarily based on current and 12 hour forecast positions published at regular intervals by NHC and JTWC (An example forecast bulletin appears as Attachment 2). A linear extrapolation between these positions to the time of an AMSU overpass provides a first-guess TC location. Adjustments of up to 1° latitude and longitude are allowable toward the warmest 54.9 GHz pixel prior to final position assignment. These assignments are critical as erroneous positioning could lead to the peak warming not being captured within the assigned field of view, resulting in underestimates of TC intensity. In a worst-case scenario, a TC path is highly non-linear (storm is recurving or accelerating), and the extrapolation technique may incorrectly forecast TC position within the satellite scan swath. Likewise, poor initial or forecast positions by the warning centers or extrapolations based on old bulletins may lead to poor positioning and inferior estimates as shown in the following example.

Cyclone Dina (10S) formed in the Southern Indian Ocean (SIO) on 17 January 2002 and strengthened as it propagated westward toward the island nation of Mauritius. The 1505 UTC AMSU pass on 21 January 2002 (Figure 15) is a good example of an improperly positioned extrapolation. The automated algorithm centers AMSU imagery on the expected TC center. At first glance, this storm is clearly incorrectly placed. The latest available forecast bulletin in this case was over 18 hours old (issued at 1800 UTC on 20 January). During that time, the TC increased in forward velocity, placing it well to the west of its forecast (extrapolated) position.
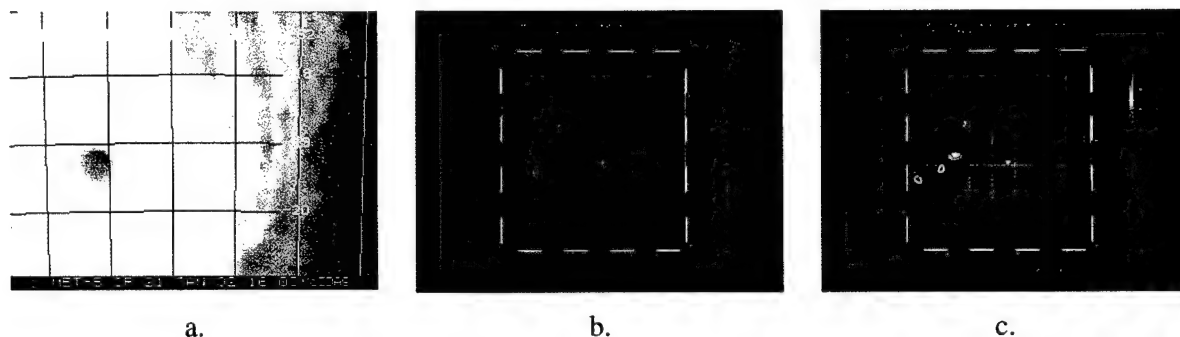

a.   b.   c.

Figure 15. Poorly extrapolated TC positions can lead to inaccurate MSLP estimates. This example depicts Cyclone Dina (10S) at 1505 UTC on 21 January 2002. Correctly positioned imagery is centered on the eye. Cyclone Dina accelerated to the west, and the extrapolated position used in this estimate was incorrectly located well east of the apparent eye. a.) GEO (METEOSAT-5) IR image. b.) AMSU-B 89.0 GHz. c.) AMSU-A channel 7 (54.9 GHz).

	Automated Estimate	Adjusted Estimate
Position	19.1° S 60.3° E	19.0° S 59.0° E
dTb7 (K)	1.23	3.72
dTb8 (K)	1.16	4.20
AMSU MSLP (hPa)	986.7	948.5

Table 10. Results of adjusting TC position for Cyclone Dina (10S) on January 21, 2002.

As a direct result of the poor forecast position, the UTWA was missed by the AMSU algorithm, and the resultant estimated intensity was too weak. The results of adjusting the storm position at the time of AMSU overpass are summarized in Table 10. Once positioned correctly, the algorithm realized an increase in dTb8 and dTb7 and an associated drop in MSLP of nearly 40 hPa. The JTWC Dvorak estimate was ~937 hPa at this time, so the adjustment to 948 hPa was a significant improvement over the automated MSLP estimate of 987 hPa.

Plans are currently underway to incorporate ATCF files to better determine storm position. These files (issued every 6 hours by the forecast centers as opposed to 12 hours for JTWC Southern Hemisphere forecast bulletins) will alleviate some of the current extrapolation problems. Manual adjustment will also remain an option with the algorithm package.

6.2. Environmental Effects

As Velden and Smith (1983) showed, a theoretical relationship exists between the UTWA and the MSLP *anomaly*. Thus, a TC embedded in an environment with lower than

normal sea level pressure (such as a monsoon trough) will produce intensities which are too weak using the current technique which is correlated with absolute MSLP values. Similarly, meridional variations in climatological environmental surface pressure become significant when TCs move successively poleward. Therefore, the relationship between the UTWA and TC intensity estimates can be dependent on the MSLP environment in which the TC is embedded. In addition, the known basin-to-basin variability in environmental MSLP and thermodynamic structures are unaccounted for in the current algorithm. All of these effects can introduce error into the MSLP estimates.

One solution is to incorporate information on the environmental surface pressure fields provided by the ATCF files. By extracting the ATCF parameter containing the mean sea level pressure assigned to the outermost isobar and adding 2 hPa, one can infer an environmental (ambient) MSLP. Subtracting the in situ MSLP (measured by aircraft), it is possible to derive an MSLP anomaly. This 'ΔMSLP' can be regressed against AMSU dTbs as described in Section 4.4 to remove variance caused by fluctuations in environmental surface pressures.

Using the ATL and EPAC cases from the dependent dataset (Table 6), ATCF-derived ΔMSLPs (outermost closed isobar + 2 hPa – observed TC MSLP) were regressed against observed temperature anomalies in both AMSU channels 7 and 8 and new relationships were derived (Figure 16).
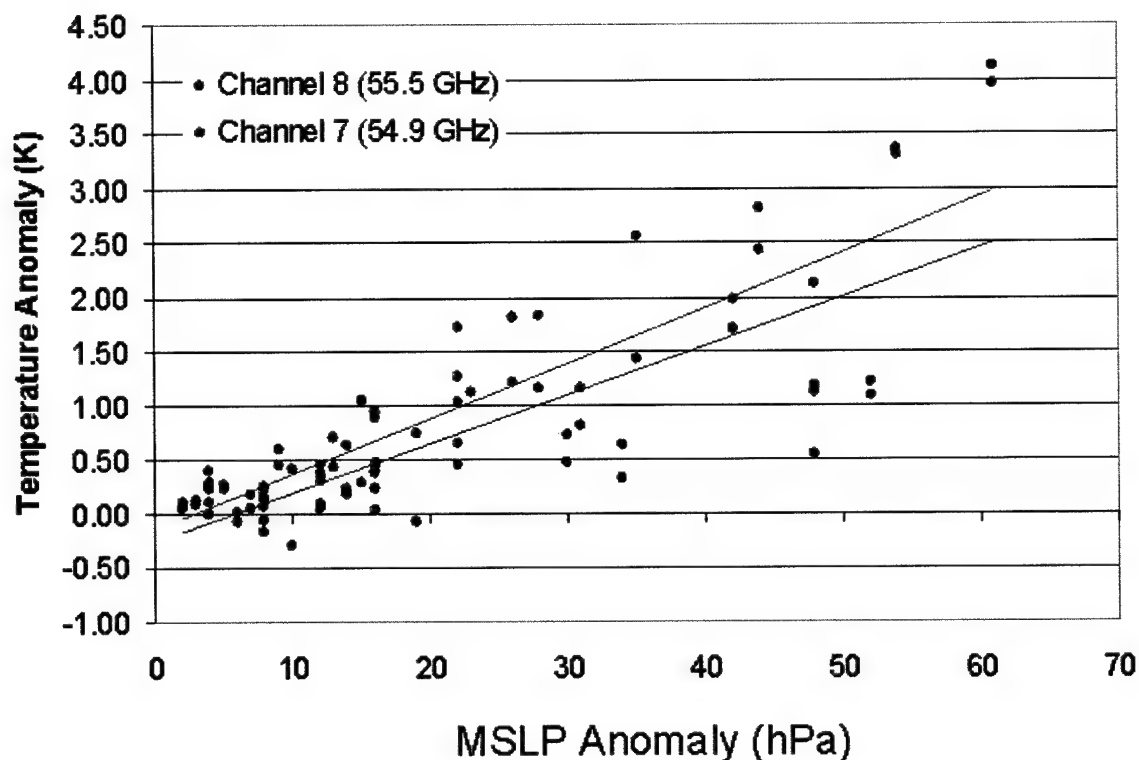
Figure 16. Statistical relationship between observed AMSU temperature anomalies and ATCF-derived ΔMSLP's. Based on 42 ATL cases.

Using the linear best-fit method applied in Section 4.4, the following solutions were derived:

$$\Delta MSLP = (dTb8 - 0.249)/(-0.045) \qquad (6)$$

$$\Delta MSLP = (dTb7 - 0.132)/(-0.051) \qquad (7)$$

Next, the multi-channel approach can be applied as follows: if dTb8>dTb7 (suspected subsampling in channel 7), ΔMSLP is determined using Equation 6. Otherwise it is calculated using Equation 7. Subtracting this quantity from the ATCF-derived environmental

surface pressure will result in a more accurate intensity estimate independent of ambient

surface pressure. Table 11 shows the results of this test.

	Multi-channel algorithm (from Table 9)	Incorporating ATCF ΔMSLPs
n	50	50
MSLP Mean Error (hPa)	7.3	7.7
MSLP Std Deviation (hPa)	5.3	5.7
Bias (hPa)	-5.5	1.8

Table 11. Effects of applying the ATCF environmental MSLP
information to the AMSU algorithm.

While the above results show little change in MSLP mean error and standard deviation,

the improvement in bias is key. Based on Equations 4 and 5 (Section 4.4), the multi-channel

approach tends to overestimate TC intensity by 5.5 hPa (MSLP too low). Including the

ATCF ancillary pressure information improves the overall bias, underestimating intensity by

only 1.8 hPa (MSLP too high). Climatologically, the average ambient pressure in the ATL

basin is roughly 1016 hPa (NHC personal communication). Inserting a temperature anomaly

of 0 K into the equation used to generate the results in the first column of Table 11 yields an

MSLP of 1011 hPa (ambient sea level pressure), while a temperature anomaly of 0 K with

ATCF information yields an environmental pressure of 1017.6 hPa. Subtracting the

respective biases results in MSLP's very close to the climatological mean. Thus, accounting

for environmental MSLP ameliorates the biases inherent in the algorithm. Figure 17

illustrates the MSLP estimate errors for each case in the independent dataset for all three

implementations: the current single-channel algorithm, the multi-channel algorithm, and the

AMSU Intensity Error Analysis

2001 Independent Dataset (n=50)

Excluding 'small eye' cases of Iris and Juliette

—— Single-channel Algorithm

—— Multi-channel Algorithm
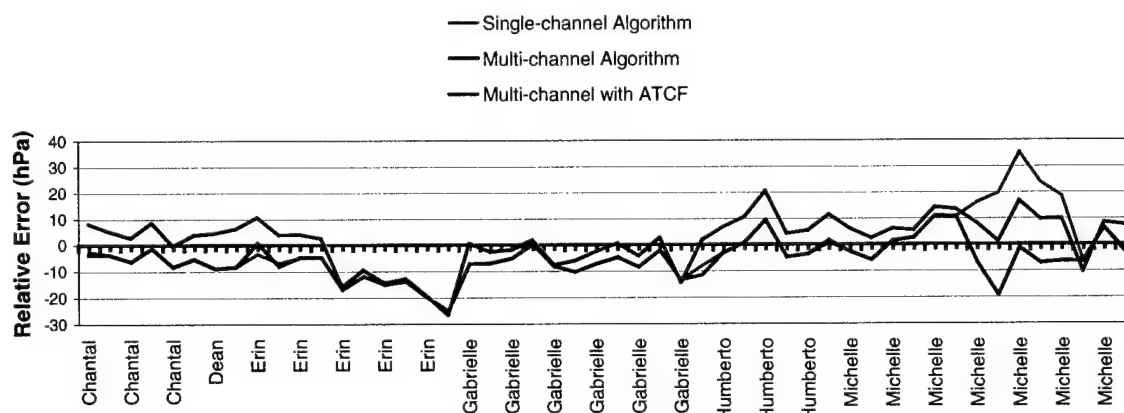
—— Multi-channel with ATCF

Figure 17. Relative case-by-case error of various AMSU intensity estimates to observed TC intensities for the 2001 independent sample excluding the small eye cases of Iris and Juliette.

multi-channel with ATCF pressure data. The plot clearly shows the low MSLP bias (TC estimate too strong) in the multi-channel approach is diminished with the inclusion of ATCF analyzed environmental MSLP fields.

To shed further light on this bias, the sample was stratified by latitude. As TCs propagate poleward, they tend to move into regimes of climatologically higher environmental MSLP. Isolating those cases in which the storms were located north of 25°N latitude produces the results shown in Table 12.

	Original multi-channel algorithm (from Table 9)	Incorporating ATCF ΔMSLPs
N	28	28
MSLP Mean Error (hPa)	8.6	7.9
MSLP Std Deviation (hPa)	5.8	6.7
Bias (hPa)	-7.4	-2.6

Table 12. Same as Table 11 except for cases poleward of 25°.

Again, the bias is significantly reduced by approximately 5 hPa by taking environmental pressures into account. We have shown that environmental pressure has a tremendous impact on the algorithm performance, and calculating TC intensity using the mean sea level pressure *anomaly* as prescribed by Velden and Smith (1983) will yield more accurate results. It is important to note that the independent dataset includes only ATL and EPAC cases where persistent synoptic-scale tropical MSLP anomalies (monsoon troughs, gyres, etc.) are less likely. The impact of including ambient pressure information would be even greater in the NWPAC basin.

6.3. Instrument Limitations

6.3.1. Horizontal Resolution

Although the AMSU is a significant improvement over its predecessors, as shown in Table 1, limitations remain. As mentioned in Section 4.2, several cases in the independent dataset were characterized by extremely compact eyes. Although characteristic of very intense storms, these 'pinholes' prove problematic for the AMSU sensor. UTWAs on the order of 24 km radius can be resolved by the AMSU 48 km horizontal resolution sensors if

they are precisely located at nadir and centered in the satellite field of view. However, any UTWA smaller than 24 km radius will be sub-sampled to some degree in raw intensity estimates and careful consideration must be given to the reliability of these cases. Although the retrieval prescribed by Merrill (1995) and Brueske (2001) is designed to account for smaller UTWAs, the method is highly dependent on accurate eyesize estimates.

The AMSU-B-derived eyesize determination technique (Section 4.2) is limited by the horizontal resolution of the sensor (16 km at nadir). The extremely compact eye of Hurricane Iris was particularly problematic during the most intense phase of her lifecycle. Aircraft reported three small concentric eyewalls, each on the order of 10 km or less in diameter (NHC 2001 Tropical Cyclone Report). While the storm trekked westward through the Caribbean, recorded MSLPs were as low as 948 hPa and sustained winds exceeded 125 knots. However, due to the extremely small UTWA, average AMSU temperature anomalies failed to exceed 0.5 K during the time of peak intensity on 8 October 2001. This is not surprising considering the relatively coarse AMSU-A resolution (48 km at nadir), but even the retrieval failed to correct for subsampling since AMSU-B was also unable to adequately resolve the extremely small eyesize.

Resolving power is not the only limiting factor in AMSU-B eyesize determination. Asymmetric eyewall convection or incomplete eyewalls will prevent determination of accurate eye radii using the method described in Section 4.2. The retrieval method, in its current form, will either assign a default eye radius if one cannot be determined or it may assign an incorrect eyesize. Once again, ATCF files contain an eyesize parameter which may provide an alternative to the AMSU-B method in certain cases. These eyesizes are obtained

by careful multi-spectral satellite analysis at the forecast centers, or in the ATL by
reconnaissance aircraft reports.

Extensive reanalysis of the entire independent dataset using ATCF eyesizes in place of 89
GHz-derived eyesizes yielded new AMSU retrieval results shown in Table 13.

	Retrieval method	Incorporating ATCF eyesize information
N	72	72
MSLP Mean Error (hPa)	11.5	8.7
MSLP Std Deviation (hPa)	12.3	7.1

Table 13. Results of including ATCF eyesize information in the current single-channel retrieval in reanalysis of the 2001 independent dataset. This particular dataset included 8 observations from Allison and Barry (2001) in addition to the complete independent dataset in Table 7.

While retrieval performance suffered during 2001 in comparison to 2000 (Table 4), the
positive contribution of including ATCF eyesize data is undeniable.

6.3.2. Instrument Noise

The noise-equivalent temperature (NEΔT) is a measure of the amount of uncertainty in
sensed brightness temperatures (radiances) due to imperfections in the sensor
instrumentation. In comparison to previous platforms (Table 1), the AMSU instrument
performs well (NEΔTs of ~0.25 K @ 290K in Channels 5-8). However, very weak TCs with
UTWAs on the order of NEΔT and smaller fall within the noise of the sensor. This was the
case for 19% of dTb7s and 28% of dTb8s in the combined dataset (n=113).

6.3.3. Weighting Functions

As demonstrated in Figure 5 and discussed in Section 2.3, the AMSU weighting

functions overlap significantly. In addition, since weighting functions are dependent on

pressure and moisture, peaks are not constrained to specific altitudes. The combined effect

leads to an uncertainty in the source altitude of sensed radiation. For example, although the

peak in the weighting function for channel 7 is in the upper troposphere, the broad 'tail' can

extend well into the lower troposphere. Therefore, temperatures from much lower in the

troposphere may on occasion make contributions to the brightness temperatures in channel 7.

Channel 8, on the other hand, peaks high enough in the troposphere to where lower-

tropospheric emissions are negligible in most situations. Having at least one "clean" channel

is another benefit of using a multi-channel approach.

6.3.4. Limb Effects

Because of the cross-track scan strategy of the AMSU instrument, radiation reaching the

sensor at higher scan angles traverses a greater depth of atmosphere. As a result, source

regions are slightly higher in altitude as scan angle increases. Assuming temperature

decreases with altitude, brightness temperatures will appear colder at higher scan angles

(limb darkening). The opposite effect is possible if the upwelling radiation passes through a

significant depth of stratosphere where temperature increases with height (limb brightening).

The algorithm in this study utilizes a NOAA/NESDIS limb correction routine, but limb

effects are not fully corrected in every situation. These effects are usually negligible (within

NEΔT) near nadir, but become greater as scan angle increases and TCs fall near the edge of the scan swath. In most cases, however, limb effects account for less than 0.25 K error after proper limb correction (Goldberg et al. 2001).

7. Qualitative Applications

In addition to providing quantitative MSLP estimates, another powerful aspect of multi-channel AMSU analysis is in qualitative use. By exploiting brightness temperature fields from channels 5-8, it is possible to gain insight into the complex thermodynamic structure of TCs and capture meteorological phenomena not immediately apparent in IR or VIS satellite imagery.

7.1. Precipitation Contamination

Deep-column convective bursts associated with overshooting tops in the TC eyewall can strongly attenuate upwelling MW radiation. If updrafts are sufficiently strong (>20 m/s), liquid and mixed phase hydrometeors may be suspended at 150 hPa and above (Joanne Simpson, NASA, personal conversation). As alluded to in Section 2.3, this situation will lead to apparent radiance cooling, and can in effect reduce the resolvable TC core warm anomaly. Diagnosing precipitation contamination is key in explaining and accounting for erroneously weak AMSU MSLP estimates in certain situations. Typhoon Tapah (01W) displayed significant attenuation just prior to intensification from a tropical storm (Figure 18a). In this example, intense convection occurs despite its apparent lack of organization in the accompanying VIS imagery. Using this diagnostic information will be a subject of an advanced AMSU retrieval approach in future work.

7.2. Aircraft Hazard Avoidance

On 20 Aug 2001, a DC-8 aircraft was on a routine reconnaissance mission over Tropical Storm Chantal in the Western Caribbean Sea. At 2250 UTC, the flight encountered significant turbulence and icing in the vicinity of 18.37°N, 86.83°W. The crew was forced to abort the mission and return to base due to cabin pressure problems. Upon close inspection of AMSU imagery, the flight path took the aircraft in the immediate vicinity of a very strong and persistent convective burst shown in the 1305 UTC radiance data (Figure 18b). This convective complex was evident for at least 9 hours prior to the incident. Although severe turbulence conditions are routinely encountered in TC environments, such long-lived convective bursts spanning hundreds of square kilometers are not. Pilots may not be able to ascertain the horizontal expanse of these phenomena once in flight, since aircraft radar are also susceptible to precipitation contamination. Had the AMSU information been available to flight planners, this aircraft incident could arguably have been avoided.

7.3. TC Transition

Because AMSU has the ability to sense discrete layers of the atmosphere, it is uniquely poised to capture the transition of a TC to an extra-tropical cyclone. Strong mid-latitude troughs are characterized by depressed tropopauses, and the resulting stratospheric undulation can be detected in channels 7 and 8 as a warm anomaly (Velden 1992). Hurricane Cindy made this transition on 31 August 1999. As shown in Figure 18c, the broad warm signature associated with the tropospheric undulation is evident in the AMSU upper

channels, while the strong UTWA continues to be reflected in the lower channels. The TC warm core and trough baroclinicity are becoming juxtaposed. Hart and Evans (2001) define the extra-tropical transition process through baroclinic forcing mechanisms. Frontolysis in the upper levels associated with a weakening temperature gradient combine with frontogenesis in the lower levels associated with strengthening temperature gradients as the baroclinic mid-latitude system "absorbs" the barotropic TC. The AMSU signature supports this description. Time series analysis of the channels 7 and 8 imagery shows a weakening temperature gradient associated with upper level frontolysis, while channels 5 and 6 show a tightening baroclinic zone (strong temperature gradient) between the TC warm core and the relatively cold signature to the northwest of the LLCC associated with low-level frontogenesis. This is a classical depiction of the beginning of extra-tropical transition.

Among the numerous distinctions between TCs and extra-tropical cyclones are amount and type of precipitation, the extent of maximum winds, propagation speed and sensible temperature patterns. This transition is important for warning centers (JTWC, NHC, AFWA, etc.) in characterizing active systems. For example, during early November 2001 a mid-latitude low pressure system persisted over the relatively warm Atlantic Ocean for two days. Eventually the system began to acquire tropical characteristics, and ship reports in the vicinity of the associated LLCC reported winds in excess of gale force. When a warm anomaly appeared in AMSU Channels 5 and 6, NHC forecasters classified the unnamed system as Hurricane Noel despite rather benign IR signatures (Figure 19). Based on apparent mid-level warming signatures, forecasters were able to infer that the thermodynamic and energetic processes (Figure 1) necessary for TC development had begun. The 11AM November 5th NHC forecast discussion referencing the imagery is included in Attachment 1.
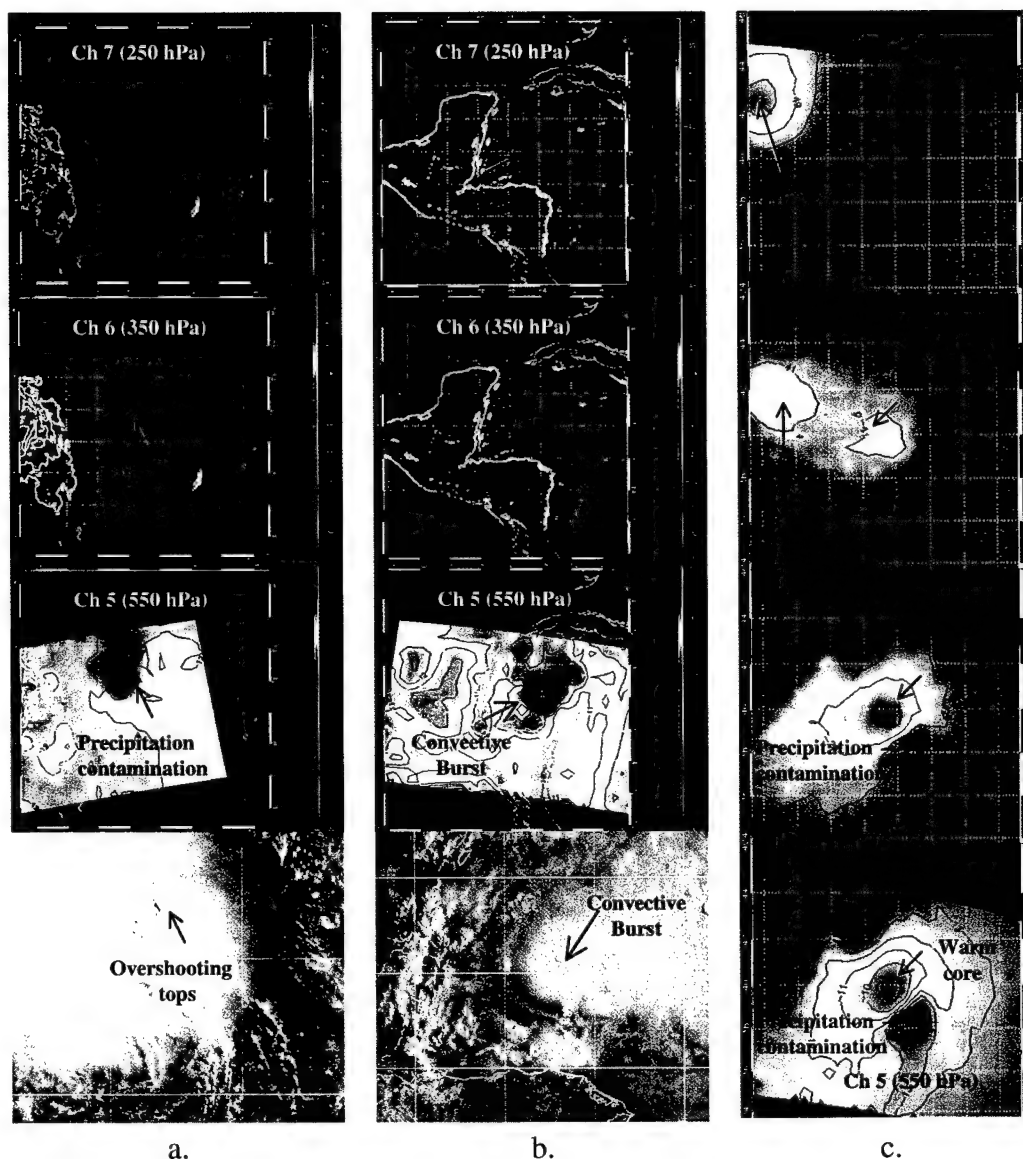
Figure 18. Qualitative applications of AMSU 53.6-55.5 GHz radiances. a.) Example of deep-column convection in Typhoon Tapah (01W) at 1041 UTC on 11 January 2002. Strong precipitation contamination in AMSU imagery is collocated with overshooting tops apparent in the accompanying visible imagery. b.) Strong convective burst in 20 August 2001 1305 UTC AMSU imagery which may have been responsible for an aircraft mishap at 2250 UTC. c.) Transition of Hurricane Cindy to an extra-tropical system. 31 August 1999 1120 UTC imagery clearly shows the very broad upper-level temperature anomaly associated with the tropopause undulation overtaking the relatively compact TC warm core in the mid-levels. Precipitation contamination southeast of the TC warm core appears in channels 5 and 6 as 'cold' anomalies. The strong temperature gradient in channel 5 and comparably weak gradient in channel 7 are indicative of transition onset (Hart and Evans 2001).
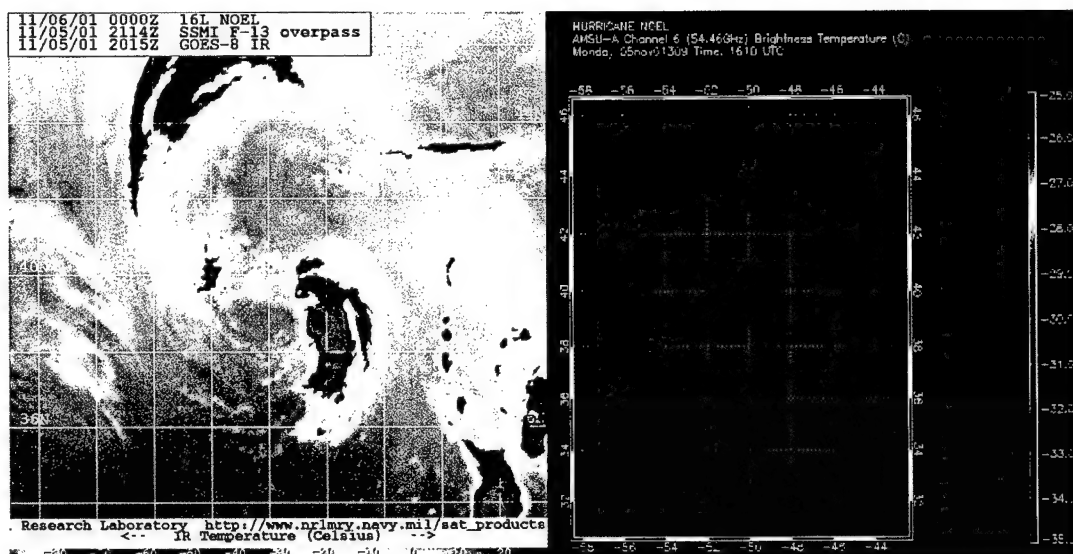
Figure 19. Transition of unnamed occluded cold-core (mid-latitude) low pressure system to Hurricane Noel at 1621 UTC on 5 November 2001. The left image shows IR signature at 2015 UTC, nearly 4 hours after NHC classified this a tropical system. The right image is the AMSU Channel 6 (weighting function peak ~350 hPa) used by warning center forecasters to identify the emerging mid-level warm core. Accompanying NHC forecast discussion appears in Attachment 1.

8. Summary and Conclusions

This research effort is an extension of Velden (1989, 1991) and Brueske (2001) to develop an objective tropical cyclone (TC) intensity estimation algorithm based on the unique capabilities of microwave remote sensing satellites. The primary goal of this research was to improve the existing AMSU TC intensity estimation algorithm through the inclusion of an additional channel. This study also attempts to quantitatively determine the impact of including ancillary environmental pressure and TC eyesize parameters in the algorithm.

Achieving this goal involved the examination of all occurrences of probable warm core (UTWA) subsampling in the single-channel (54.9 GHz) model and bringing in additional information from a second AMSU channel (55.5 GHz) to re-calculate the final intensity estimates. A logical multi-channel algorithm was developed from a two-year sample (1999-2000) and applied to an independent sample of TCs (2001) in a fully-automated routine. Four case studies were presented to illustrate the strengths of the multi-channel algorithm.

The second half of this study examined the impact of adding auxiliary information provided by Automated Tropical Cyclone Forecast (ATCF) datafiles in reducing the bias inherent in the current model. A scheme was developed to extract environmental (ambient) surface pressures to reexamine the relationship between AMSU temperature anomalies and observed MSLP *anomalies*. Additionally, an eyesize parameter provided by the ATCF was examined as an input field into the forward model (retrieval).

The results presented in this paper suggest an operational multi-channel approach to TC intensity estimation is not only feasible, but prudent. This research demonstrates that AMSU MSLP estimate mean errors and standard deviations can be reduced significantly by

including an additional AMSU channel in certain well-characterized situations. In addition, bias can be significantly reduced through inclusion of ATCF pressure fields, which address the issue of environmental variability. A summary of the quantitative results of this progression appear in Table 14.

	Single-channel Algorithm	Multi-channel Algorithm	Multi-channel Algorithm using ΔMSLP (ATCF)
N	50	50	50
MSLP Mean Error (hPa):	8.69	7.30	7.73
MSLP Std Dev (hPa):	7.17	5.34	5.72
MSLP Bias (hPa):	-2.41	-5.51	1.83

Table 14. Summary of major findings. The existing single-channel AMSU algorithm (col. 1) was supplemented with information from a second channel (col. 2). Mean error and standard deviation were significantly reduced, but the multi-channel algorithm exhibited more bias (TC's estimates were too intense by 5.5 hPa). Calculation of the MSLP anomaly (ΔMSLP) using ATCF information and regressing this parameter against the multi-channel AMSU UTWA significantly reduced this bias (col. 3).

The final phase of this research involved re-analyzing the independent dataset and replacing 89.0 GHz-derived eyesizes with those published in ATCF files for input into the AMSU algorithm retrieval. Inclusion of the ancillary information dramatically improved retrieval performance, validating Merrill's hypothesis on eyesize sensitivity (1995). Reanalysis using new eyesizes reduced MSLP mean error by 2.8 hPa and standard deviation by 5.2 hPa.

While promising, these results indicate limitations still exist with this technique. The impact of intense precipitation can lead to anomalous "cooling" of the AMSU radiance and UTWA fields, which is inherently difficult to account for. The relatively coarse horizontal

resolution as well as certain effects due to satellite scan geometry can limit the use of the technique in storms with very small eyes (and corresponding UTWAs).

This study detailed three very specific qualitative applications in which AMSU temperature fields can aid in general meteorological and operational analysis. Otherwise considered "noise" in the TC intensity estimation process, precipitation signals provide considerable information regarding the convective structure of tropical systems, particularly where IR and VIS imagery cannot. Also, AMSU data can be utilized to identify and characterize critical transitions from tropical to extra-tropical systems and visa versa.

The addition of NOAA-16 AMSU data during the 2001 season virtually doubled the existing database of MSLP-UTWA observations. With two operational AMSU instruments in LEO, it is now possible to capture up to 4-6 scenes per TC per day depending on storm location (Section 2.2). With the impending launch of new AMSU sensors on NOAA-17 and Aqua platforms in 2002, the available dataset used to train the multi-channel algorithm will continue to grow. Increasing temporal resolution of the data will fill in critical gaps between forecast advisories. Until high-resolution geostationary microwave sensors are viable, the polar-orbiting AMSU will continue to provide a unique perspective into TC thermodynamic structure.

The UW-CIMSS TC intensity estimation algorithm is currently being transformed to be fully portable for eventual integration into forecast centers. Continuing to exploit the entire MW spectrum, future work will incorporate Channels 5-6 and attempt to explicitly treat precipitation effects. The research presented in this thesis serves as an important stepping stone toward the ultimate goal: a fully-operational, integrated AMSU TC intensity estimation algorithm that uses multiple channels and a physical retrieval of the eye to hydrostatically

calculate TC MSLP. Merging the AMSU technique with the IR-based Objective Dvorak Technique and additional sensors like the Defense Meteorological Satellite System Special Sensor Microwave Imager (DMSP-SSMI) and future NPOESS platforms will provide operational forecasters with a single tool which objectively accounts for the numerous complexities of TC physical and thermodynamic structure.

Attachment 1

ZCZC MIATCDAT1 ALL
TTAA00 KNHC DDHHMM
HURRICANE NOEL SPECIAL DISCUSSION NUMBER   1
NATIONAL WEATHER SERVICE MIAMI FL
11 AM EST MON NOV 05 2001

SHIP WRYG REPORTED 65 KT WINDS IN THE SOUTHEAST QUADRANT OF THE LOW
ABOUT 60 NM FROM THE CENTER. THE SYSTEM HAS A BROKEN RING OF
CONVECTION REASONABLY NEAR THE CENTER...AND HAS A WEAK MID-LEVEL
WARM SIGNATURE IN THE MOST RECENT AMSU DATA FROM THE CIMSS WEB PAGE.
ON THIS BASIS THE SYSTEM IS CONSIDERED A HURRICANE AND ADVISORIES
ARE INITIATED.

NOEL IS MOVING AT 360/10 AHEAD OF A LARGE MID-LEVEL CUTOFF LOW
CURRENTLY OVER NEW ENGLAND. NOEL IS EXPECTED TO CONTINUE ON THIS
GENERAL PATH WITH SOME ACCELERATION AS A SEPARATE EXTRATROPICAL
CYCLONE STRENGTHENS SOUTHEAST OF NOVA SCOTIA OVER THE NEXT 24 HOURS.
NOEL SHOULD EVENTUALLY GET ABSORBED BY THIS EXTRATROPICAL LOW...BUT
LIKELY AFTER BECOMING EXTRATROPICAL ITSELF AS IT BEGINS TO MOVE OVER
MUCH COLDER WATERS. THE OFFICIAL FORECAST IS A BLEND OF THE AVN AND
UKMET SOLUTIONS...AND INDICATES THAT THE SYSTEM COULD PASS CLOSE
ENOUGH TO EASTERN NEWFOUNDLAND TO BRING TROPICAL STORM FORCE WINDS
THERE.

FORECASTER FRANKLIN

FORECAST POSITIONS AND MAX WINDS

INITIAL   05/1600Z 38.5N 50.4W   65 KTS
12HR VT   06/0000Z 40.0N 50.4W   65 KTS
24HR VT   06/1200Z 44.0N 51.0W   60 KTS...BECOMING EXTRATROPICAL
36HR VT   07/0000Z 51.0N 50.0W   55 KTS...EXTRATROPICAL
48HR VT   07/1200Z...ABSORBED

Attachment 2

WTPN31 PGTW 281500   2002059 1416
1. TROPICAL STORM (TS) 02W (MITAG) WARNING NR 008
  01 ACTIVE TROPICAL CYCLONE IN NORTHWESTPAC
  MAX SUSTAINED WINDS BASED ON ONE-MINUTE AVERAGE

  WARNING POSITION:
  281200Z3 --- NEAR 7.2N9 152.0E8
    MOVEMENT PAST SIX HOURS - 280 DEGREES AT 11 KTS
    POSITION ACCURATE TO WITHIN 060 NM
    POSITION BASED ON CENTER LOCATED BY SATELLITE
  PRESENT WIND DISTRIBUTION:
  MAX SUSTAINED WINDS - 040 KT, GUSTS 050 KT
  RADIUS OF 035 KT WINDS - 055 NM NORTHEAST QUADRANT
                OVER WATER
            045 NM SOUTHEAST QUADRANT
                OVER WATER
            045 NM SOUTHWEST QUADRANT
            055 NM NORTHWEST QUADRANT
                OVER WATER
  REPEAT POSIT: 7.2N9 152.0E8

  FORECASTS:
  12 HRS, VALID AT:
  010000Z1 --- 7.5N2 149.6E0
  MAX SUSTAINED WINDS - 045 KT, GUSTS 055 KT
  RADIUS OF 035 KT WINDS - 060 NM NORTHEAST QUADRANT
            050 NM SOUTHEAST QUADRANT
            050 NM SOUTHWEST QUADRANT
                OVER WATER
            060 NM NORTHWEST QUADRANT
                OVER WATER
  VECTOR TO 24 HR POSIT: 275 DEG/ 12 KTS
  ---
  24 HRS, VALID AT:
  011200Z4 --- 7.6N3 147.2E4
  MAX SUSTAINED WINDS - 050 KT, GUSTS 065 KT
  RADIUS OF 035 KT WINDS - 070 NM NORTHEAST QUADRANT
            055 NM SOUTHEAST QUADRANT
            055 NM SOUTHWEST QUADRANT
            070 NM NORTHWEST QUADRANT
  VECTOR TO 36 HR POSIT: 275 DEG/ 12 KTS
  ---
  36 HRS, VALID AT:
  020000Z2 --- 7.8N5 144.7E6
  MAX SUSTAINED WINDS - 060 KT, GUSTS 075 KT
  RADIUS OF 050 KT WINDS - 025 NM
  RADIUS OF 035 KT WINDS - 075 NM NORTHEAST QUADRANT
            060 NM SOUTHEAST QUADRANT
            060 NM SOUTHWEST QUADRANT
                OVER WATER
            075 NM NORTHWEST QUADRANT
  VECTOR TO 48 HR POSIT: 285 DEG/ 12 KTS

  EXTENDED OUTLOOK:
  48 HRS, VALID AT:
  021200Z5 --- 8.5N3 142.3E0
  MAX SUSTAINED WINDS - 065 KT, GUSTS 080 KT
  RADIUS OF 050 KT WINDS - 035 NM
  RADIUS OF 035 KT WINDS - 095 NM NORTHEAST QUADRANT
            075 NM SOUTHEAST QUADRANT
            075 NM SOUTHWEST QUADRANT
            095 NM NORTHWEST QUADRANT
  VECTOR TO 72 HR POSIT: 290 DEG/ 13 KTS
  ---
  72 HRS, VALID AT:
  031200Z6 --- 10.3N4 137.5E6
  MAX SUSTAINED WINDS - 075 KT, GUSTS 090 KT
  RADIUS OF 050 KT WINDS - 040 NM
  RADIUS OF 035 KT WINDS - 110 NM NORTHEAST QUADRANT
            090 NM SOUTHEAST QUADRANT
            090 NM SOUTHWEST QUADRANT
            110 NM NORTHWEST QUADRANT

  REMARKS:
  281500Z6 POSITION NEAR 7.3N0 151.4E1.
  TROPICAL STORM (TS) 02W (MITAG), LOCATED APPROXIMATELY 17 NM
  SOUTHEAST OF
  CHUUK, HAS TRACKED WESTWARD AT 11 KNOTS DURING THE PAST 6 HOURS. THE
  WARNING POSITION IS BASED ON 281130Z5 INFRARED SATELLITE IMAGERY AND
  AVAILABLE SYNOPTIC DATA. THE WARNING INTENSITY IS BASED ON SATELLITE
  CURRENT INTENSITY ESTIMATES OF 35 AND 45 KNOTS AND SYNOPTIC DATA.
  MAXIMUM SIGNIFICANT WAVE HEIGHT AT 281200Z3 IS 16 FEET. REFER TO
  WWPW31 RJTX FOR ADDITIONAL SEA HEIGHT INFORMATION. NEXT WARNINGS AT
  282100Z3, 010300Z4, 010900Z0 AND 011500Z7.

List of Acronyms

AFWA	Air Force Weather Agency
AMSU	Advanced Microwave Sounding Unit
ATCF	Automated Tropical Cyclone Forecasting system
ATL	Atlantic
CDAS	Command and Data Acquisition Station
CIMSS	Cooperative Institute of Meteorological Satellite Studies
DMSP	Defense Meteorological Satellite Program
dTb	Brightness Temperature Anomaly
dTb7	AMSU Channel 7 (54.9 GHz) Temperature Anomaly
dTb8	AMSU Channel 8 (55.5 GHz) Temperature Anomaly
DTG	Date-Time Group
EM	Electromagnetic
EPAC	Eastern Pacific
GEO	Geostationary Earth Orbit
GMS	Geostationary Meteorological Satellite (Japan)
GMT	Greenwich Meridian Time
IO	Indian Ocean
IR	Infrared
JTWC	Joint Typhoon Warning Center
LEO	Low Earth Orbit
LLCC	Low-level Circulation Center
MSLP	Minimum Sea Level Pressure
MSU	Microwave Sounding Unit
MW	Microwave
NESDIS	National Environmental Satellite, Data, and Information Service
NH	Northern Hemisphere
NHC	National Hurricane Center
NOAA	National Oceanic and Atmospheric Administration
NWPAC	Northern West Pacific
NPOESS	National Polar-orbiting Operational Environmental Satellite System
SCAMS	Scanning Microwave Spectrometer
SH	Southern Hemisphere

SSMI	Special Sensor Microwave Imager
TAFB	Tropical Analysis and Forecast Branch (NOAA)
Tb	Brightness Temperature
TC	Tropical Cyclone
USAF	United States Air Force
UTC	Coordinated Universal Time
UTWA	Upper Troposphere Warm Anomaly
UW	University of Wisconsin - Madison
VIS	Visible satellite imagery
WWII	World War II (1939-1945)

References

Adler, R.F. and E.B. Rodgers, 1977: Satellite-observed latent heat release in tropical cyclones *Monthly Weather Review*, **105**, 956-963.

Brueske, Kurt F., 2001: Satellite-based tropical cyclone intensity estimations using NOAA-KLM advanced microwave sounding unit (AMSU) data. PhD dissertation, 106 leaves.

Brueske, Kurt F., and Christopher S. Velden, 2002: Satellite-based tropical cyclone intensity estimation using AMSU. Accepted in *Monthly Weather Review*.

Dvorak, V.F., 1975: Tropical cyclone intensity analysis and forecasting from satellite imagery. *Monthly Weather Review*, **103**, 420-430.

Emanuel, Kerry, 2000: A statistical analysis of tropical cyclone intensity. *Monthly Weather Review*, **128**, 1139-1152.

Ferraro, R.R., S.J. Kusselson, and M.C. Colton, 1998: An introduction to passive microwave remote sensing and its applications. *National Weather Digest*, **22**, 11-23.

Fuller, R.F., 1990: Thor's Legions: Weather Support to the U.S. Air Force and Army 1937-1987. American Meteorological Society, 443 pp.

Goldberg, Mitchell D., David S. Crosby and Lihang Zhou, 2001: The limb adjustment of AMSU-A observations: methodology and validation. *Journal of Applied Meteorology*, Boston, MA, **40**(1): 70-83, January 2001. Refs., figs., table. DAS, DLC.

Gray, William M., 1979: Tropical cyclone intensity determination through upper-tropospheric aircraft reconnaissance. *Bulletin of the American Meteorological Society*, Volume 60, No. 9, 1069-1074.

Hart, R. E., and J. L. Evans, 2001: A climatology of extratropical transition of Atlantic tropical cyclones. *J. Climate*, **14**, 546-564.

Kidder, Stanley Q., William M. Gray and Thomas H. Vonder Haar, 1978: Estimating tropical cyclone central pressure and outer winds from satellite microwave data. *Monthly Weather Review*, **106**, 1458-1464.

Kidder, Stanley Q., 1979: Determination of tropical cyclone surface pressure and winds from satellite microwave data. Atmospheric Science Paper, No. 307, 87 pp. (PhD dissertation).

Kidder, Stanley Q., Mitchell D. Goldberg, Raymond M. Zehr, Mark DeMaria, James F. W. Purdom, Christopher S. Velden, Norman C. Grody, and Sheldon J. Kusselson, 2000: Satellite Analysis of Tropical Cyclones Using the Advanced Microwave Sounding Unit (AMSU). *Bulletin of the American Meteorological Society*, **81**, No. 6, 1241-1260.

Klein, Peter M., Patrick A. Harr, and Russell L. Elsberry, 2000: Extratropical Transition of Western North Pacific Tropical Cyclones: An Overview and Conceptual Model of the Transformation Stage. *Weather and Forecasting*, **15**, Number 4, 373-396.

Knaff, John A., Raymond M. Zehr, Mitchell D. Goldberg and Stanley Q. Kidder, 2000: An example of temperature structure differences in two cyclone systems derived from the advanced microwave sounder unit. *Weather and Forecasting*, **15**, 476-483.

Landsea, Christopher, 1989: A record minimum seal level pressure observed in Hurricane Gilbert. *Monthly Weather Review*, **117**, Notes and correspondence, 2824-2828.

Merrill, R. T., 1994: Typhoon Monitoring Using Passive Microwave Observations. PL-TR-95-2012

Merrill, R. T., 1995: Simulations of Physical Retrieval of Tropical Cyclone Thermal Structure Using 55-GHz Band Passive Microwave Observations from Polor-Orbiting Satellites. *Journal of Applied Meteorology*, **34**, 773-778.

NOAA-KLM Online User's Guide: http://www2.ncdc.noaa.gov/docs/klm .

Spenser, Roy W. and William D. Braswell, 2001: Atlantic tropical cyclone monitoring with AMSU-A: Estimation of maximum sustained wind speeds. *Monthly Weather Review*, **129**, 1518-1532.

Velden, Christopher S., 1982: Monitoring tropical cyclone evolution with NOAA satellite microwave observations. M.S. thesis, 78 leaves.

Velden, Christopher S. and W.L. Smith, 1983: Monitoring tropical cyclone evolution with NOAA satellite microwave observations. *Journal of Climate and Applied Meteorology*, **22**, 714-724.

Velden, Christopher S., 1989: Observational analyses of North Atlantic tropical cyclones from NOAA satellite microwave observations. *Journal of Applied Meteorology*, **28**, 59-70.

Velden, Christopher S., Brian Goodman and Robert T. Merrill, 1991: Western North Pacific tropical cyclone intensity estimation from NOAA Polar-Orbiting satellite microwave data. *Monthly Weather Review*, **119**, 159-168.

Velden, Christopher S., 1992: Satellite-based microwave observations of tropopause-level thermal anomalies: qualitative applications in extratropical cyclone events. *Weather and Forecasting, 7*, 669–682.

Velden, Christopher S., and Kurt F. Brueske, 1999: Application of AMSU-A radiance fields and retrievals to the analysis of hurricanes. P3.1 for 10th Conf. on Sat. Met.

Weatherford, C. L., and W. M. Gray, 1988: Typhoon structure as revealed by aircraft reconnaissance. Part I: Data analysis and climatology. *Monthly Weather Review*, **119**, 1032-1043.

Weatherford, C. L., and W. M. Gray, 1988: Typhoon structure as revealed by aircraft reconnaissance. Part II: Structural variability. *Monthly Weather Review*, **119**, 1044-1056.